Universiteit Utrecht

Physics and Astronomy

Constraining the electric charge of binary black holes and neutron stars through gravitational wave observations

Bachelor Thesis

Thomas F.M. Spieksma

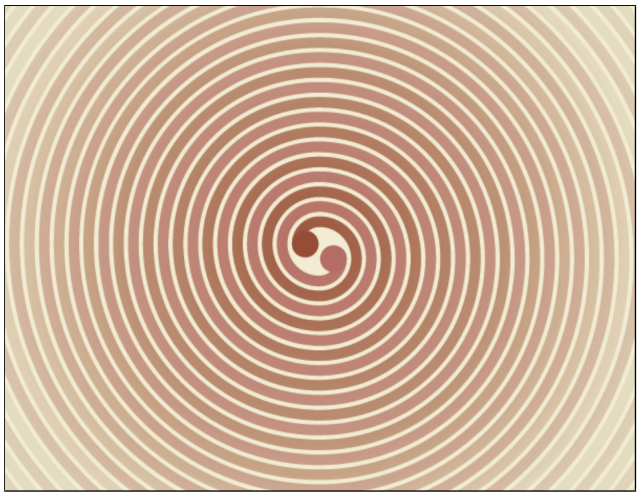

Figure taken from International Centre for Theoretical Physics [1]

Supervisor:

Prof. Dr. C.F.F. van den Broeck
Universiteit Utrecht/Nikhef

June 10, 2020

Abstract

Gravitational wave observations provide new possibilities to explore the Universe. A promising area for gravitational wave physics is compact binary systems consisting of black holes or neutron stars. Both are generally expected to be electrically neutral to good approximation, however general relativity does not prohibit either to possess a net electric charge. Should there be a significant electric charge present in a binary system, this would influence the orbital motion and consequently be noticeable through gravitational wave analysis.

In this thesis, we lay down the groundwork for gravitational waves from binary systems and motivate how electric charges can be accreted by black holes. We derive the additional energy and radiated power terms induced by the charges and determine how these influence the gravitational waveform. We find that there is a -1 post-Newtonian term that includes a relative electric charge difference and can only take on non-positive values. Furthermore, using data from five binary black hole events, we produce probability distributions of the -1 post-Newtonian term. None of the events show signs of a significant relative charge difference. We estimate 90% upper bounds on the dimensionless relative charge difference of the binaries which are all in the order of 10^{-1}. From here, we move on to the double pulsar PSR J0737-3039. Through radio observations, we again estimate an upper bound on the dimensionless relative charge difference, which turns out to be in the order of 10^{-3}. Finally, we adopt the Fisher matrix formalism to derive future bounds on black hole binaries that can potentially be reached once the Einstein Telescope becomes active.

Contents

Prologue

When Edwin A. Abbott wrote his renowned novel *Flatland* in 1884, he described the encounter between the two-dimensional world of a square and the three-dimensional world of a sphere. One day, the sphere visited the square in its two-dimensional world and the square could naturally only see a circle. Then, the sphere pursued by flaunting his three-dimensional properties, levitating up and down through the two-dimensional world. This allowed the square to see an expanding and contracting circle. When the square asked if there were even more dimensions, the sphere got angry as it would surely be in the highest dimensional world.

At first, this story was not a successful one. However, after Einstein published his paper on general relativity in 1915, physicists saw this story as a way to explain the extra fourth dimension Einstein introduced. From his theory, the prediction of gravitational waves arose. Their detection opened up a new era in physics. In a way, we stepped into a new dimension where we can open our ears and listen to the Universe.

Introduction

A little over a 100 years ago, Albert Einstein put his last hand to the theory of general relativity (GR). He described how mass and spacetime are in a tight relationship where mass distorts spacetime and in turn spacetime dictates mass how to move. GR has shaped our entire view of the Universe and it has proven to be one of the most substantial theories in physics. Time and time again, physicists have tested, argued and discussed GR and time and time again it has persevered. On the 14th of September 2015 yet another confirmation emerged: the first direct observation of gravitational waves [2]. Previously, indirect observations were already made in 1974 by Hulse and Taylor [3], whose measurements on the changes in orbital motion of a binary pulsar were extremely consistent with the emission of gravitational waves. However, the implications of the existence of gravitational waves extend further than just confirming Einstein's predictions. It provides (astro)physicists with a new, independent way of measuring known phenomena in the Universe and may even lead to the discovery of yet unknown phenomena.

In this thesis, we are going to investigate the intriguing possibility of black holes and neutron stars possessing some net electric charge. In general, both are treated as electrically neutral, but GR does not prohibit either to have a net electric charge. When such objects are part of a binary system, the effects of a significant net electric charge should come forward. Specifically, the way the two objects spiral towards each other will be determined not just by the gravitational wave radiation, but also by electromagnetic dipole radiation. As there is currently no observational evidence for a significant net electric charge in compact binary systems, we do assume the effects of electric charges to be small. In particular, throughout this thesis we will only consider the contribution of electric charge up to leading order. Recently discovered gravitational wave events will allow us to put constraints on a certain parameter linked with dipolar emission. We will assume that this dipolar emission originates from the presence of electric charges and therefore our research question will be:

Can we estimate upper bounds on the electric charge of binary black holes and binary neutron stars through gravitational wave observations?

We will start off at Chapter 1 with a short introduction on gravitational waves in general, after which we will focus our discussion onto binaries in Chapter 2. Next, we will look into possible mechanisms that allow black holes to acquire electric charges in Chapter 3. Then, in Chapter 4, we will look at the effect of these charges on the gravitational waveform and afterwards use gravitational wave observations to set bounds on the electric charge of binary black hole events in Chapter 5. Thereafter, in Chapter 6, we will consider a similar procedure, but then applied to a binary neutron star, specifically the double pulsar. In Chapter 7, we will use the Fisher matrix formalism to estimate future bounds that can be set once the Einstein Telescope will become active and finally, in Chapter 8, we will end with some concluding remarks.

1 Gravitational waves and their detection

In this chapter, we will give a brief introduction on gravitational waves (GWs) and the way they are detected. This should in no way be regarded as a full description of GWs, as some important steps and derivations are left out in order to keep an overview. Nevertheless, the relevant terminology, equations and concepts that are needed to follow this thesis, will be addressed. If the reader has never dealt with GWs before, it might be useful to exploit the corresponding references in this chapter.

We will first discuss linearised gravity in Section 1.1, then we will shortly address the energy GWs carry in Section 1.2. Next, in Section 1.3, we will write down the quadrupole formula and finally, in Section 1.4, we will outline how GWs are detected.

1.1 Linearised gravity

The Einstein field equations (EFE), which were first written down in the theory of general relativity [4], are hard to solve exactly due to their highly non-linear nature. Fortunately, we can study the properties of GWs in the so-called weak-field approximation. In this approximation, we assume that far from gravitating matter, the gravitational field is weak and we can do a linear expansion of the EFE around the flat Minkowski space metric. Therefore we can write the metric tensor as:

$$g_{\mu\nu} = \eta_{\mu\nu} + h_{\mu\nu}, \tag{1.1}$$

where $\eta_{\mu\nu}$ is the Minkowski metric and $h_{\mu\nu} \ll 1$ is a small metric perturbation.

The linearised EFE are gauge-invariant and this gauge freedom can be used to simplify the form of the field equations. Through a process which we will not derive here (see e.g. [5]), the linearised field equations in the Lorentz gauge reduce to:

$$\Box \bar{h}_{\mu\nu} = -\frac{16\pi G}{c^4} T_{\mu\nu}, \tag{1.2}$$

where $\bar{h}_{\mu\nu} = h_{\mu\nu} - (1/2)\eta_{\mu\nu} h^{\alpha}_{\alpha}$, $\Box$ represents the d'Alembertian operator, G is the Newtonian gravitational constant, c is the speed of light and $T_{\mu\nu}$ is the stress-energy tensor. In vacuum, i.e. $T_{\mu\nu} = 0$, the linearised field equations reduce to:

$$\Box \bar{h}_{\mu\nu} = 0. \tag{1.3}$$

Writing out the d'Alembertian operator in full, shows that this is the classic wave equation with propagation velocity c :

$$\frac{\partial^2 \bar{h}_{\mu\nu}}{\partial t^2} = c^2 \left(\frac{\partial^2 \bar{h}_{\mu\nu}}{\partial x^2} + \frac{\partial^2 \bar{h}_{\mu\nu}}{\partial y^2} + \frac{\partial^2 \bar{h}_{\mu\nu}}{\partial z^2} \right). \tag{1.4}$$

As there is still some gauge freedom left in Eq. (1.2), we are going to impose another gauge condition. Most commonly used is the transverse-traceless (TT) gauge, which ensures that the metric perturbation is perpendicular to the direction of propagation and also traceless [5]. The TT gauge is very convenient, as it fully fixes all the local gauge freedom. The metric perturbation that we are then left with, only contains physical, non-gauge information about the GW radiation. When we consider a plane wave propagating in the z-direction, the metric perturbation can be written as [1]:

$$h^{TT}_{ij} = \begin{pmatrix} h_+ & h_\times & 0 \\ h_+ & -h_\times & 0 \\ 0 & 0 & 0 \end{pmatrix} \cos\left(\omega(t - z/c)\right), \tag{1.5}$$

where h_+ and $h_\times$ are the plus and cross polarization. They represent the two possible degrees of freedom a GW has.

[1] Since the metric perturbation is traceless, there is no distinction anymore between $\bar{h}^{TT}_{ij}$ and h^{TT}_{ij}, moreover note that in the TT gauge the metric perturbation only has spatial components.

1.2 Energy in gravitational waves

The question whether GWs carry energy has been up for debate in the past. It is a tricky subject, as GWs themselves are curvatures in spacetime, yet if they carry energy they should also cause an additional spacetime curvature. To derive what this extra curvature looks like, we would have to go beyond linear order (at least quadratic order in $h_{\mu\nu}$). As locally we can always choose a coordinate system for one point in which the metric is just the Minkowski metric ($h_{\mu\nu} = 0$) and also the first derivative of $h_{\mu\nu}$ is 0, we can already say, without carrying out the explicit calculation, that there should be a an average involved [6].

The EFE can be split up in a low and high frequency part, where the high frequency part describes the GWs and the low frequency part describes the background. We are interested in the effect on the background and we will write the low-frequency EFE as follows [7]:

$$\bar{R}_{\mu\nu} - \frac{1}{2}\bar{g}_{\mu\nu}\bar{R} = \frac{8\pi G}{c^4}\left(\bar{T}_{\mu\nu} + t_{\mu\nu}\right), \tag{1.6}$$

where the bars indicate the low-frequency part, $R_{\mu\nu}$ represents the Ricci tensor, R the Ricci scalar and $t_{\mu\nu}$ is an additional stress-energy tensor given by:

$$t_{\mu\nu} = -\frac{c^4}{8\pi G}\left\langle R^{(2)}_{\mu\nu} - \frac{1}{2}\bar{g}_{\mu\nu}R^{(2)}\right\rangle, \tag{1.7}$$

where the (2) denotes the quadratic order in $h_{\mu\nu}$.

This additional stress-energy tensor is the result of the additional spacetime curvature caused by the GWs. Writing out the components of the Ricci tensor and the Ricci scalar in Eq. (1.7), this will reduce to [7]:

$$t_{\mu\nu} = \frac{c^4}{32\pi G}\left\langle \partial_\mu h_{\alpha\beta}\partial_\nu h^{\alpha\beta}\right\rangle. \tag{1.8}$$

Finally, this can be transformed into a more convenient expression for the GW energy passing through some sphere $\mathcal{S}$ per unit time [7]:

$$\frac{dE_{\mathrm{GW}}}{dt} = \frac{c^3 r^2}{16\pi G}\int_{\mathcal{S}} d\Omega \left\langle \dot{h}_+^2 + \dot{h}_\times^2\right\rangle. \tag{1.9}$$

1.3 The quadrupole formula

In Eq. (1.4), we saw that the linearised field equations had wave solutions in vacuum, however, we now want to obtain a general solution to the linearised field equations given by Eq. (1.2). By using the proper Green's function, the general solution outside the source in the TT gauge is given as follows [8]:

$$h_{ij}^{TT}(t,\vec{x}) = \frac{4G}{c^2}\Lambda_{ij,kl}(\hat{\vec{n}})\int_{\mathcal{V}} d^3\vec{x}'\frac{1}{|\vec{x}-\vec{x}'|}T_{kl}(t - \frac{|\vec{x}-\vec{x}'|}{c}, \vec{x}'), \tag{1.10}$$

where the integral is taken over a volume $\mathcal{V}$ containing the source, $\Lambda_{ij,kl}$ is the projection operator onto the TT gauge, $\hat{\vec{n}}$ is the unit vector perpendicular to the wavefront and $|\vec{x}-\vec{x'}|$ is the distance from the source to the observer. For non-relativistic sources, this can be further reduced to an equation for the mass quadrupole radiation formula, which is given by:

$$[h_{ij}^{TT}(t,\vec{x})]_{\mathrm{quad}} = \frac{2G}{c^2 r}\Lambda_{ij,kl}(\hat{\vec{n}})\ddot{M}^{k\ell}(t - r/c), \tag{1.11}$$

where r has taken the place of $|\vec{x}-\vec{x}'|$ as we are interested in h_{ij}^{TT} at large distances from the source (where our detectors are located) and $M^{k\ell}$ is the mass quadrupole moment given by:

$$M^{k\ell} = \frac{1}{c^2}\int d^3\vec{x}\, T^{00}(t,\vec{x})x^k x^\ell. \tag{1.12}$$

The mass quadrupole moment is the leading order term for the radiation of GWs, as there is no mono- or dipole GW radiation in GR due to the conservation of the stress-energy tensor [8].

Without loss of generality, we can set the propagation direction to the z-direction and deduce from Eq. (1.5) and Eq. (1.11) what the two different polarization states, h_+ and $h_\times$, are in terms of the mass quadrupole moment:

$$h_+ = \frac{1}{r}\frac{G}{c^4}(\ddot{M}_{11} - \ddot{M}_{22}), \tag{1.13}$$

$$h_\times = \frac{2}{r}\frac{G}{c^4}\ddot{M}_{12}. \tag{1.14}$$

1.4 Detections of gravitational waves

The first direct observations of GWs were made with the Advanced LIGO detectors [2]. These detectors consist of two large interferometers, one located in Livingston (Louisiana) and the other one located in Hanford (Washington). Due to their geographical distance, an incoherent glitch caused by seismic disturbances at one site can be better distinguished from a coherent signal of a GW passing through both detectors. The interferometers consist of two arms of 4 km long, perpendicular to each other. A schematic overview of the set-up is given in Fig. 1. When an incoming laser beam passes through a beam splitter, the beam will be split up and sent down both arms of the interferometer. At the end of those arms, there is a mirror suspended as a pendulum which reflects the beam. The Advanced LIGO detectors (the Advanced Virgo detector located in Italy works in the same way) are tuned in such a way that the two laser beams will rejoin in total destructive interference. A GW passing through the detector will lengthen one arm and shorten the other, depending on the strength of the different polarisation states and the angle of incidence on the detector. The changed length of the arms means the laser beam will have to travel slightly longer or shorter. This changes the interference pattern when the beams rejoin and that is what a photodiode will measure. There is a whole range of subtleties involved in the real set-up [9], but this is the simplified overview.

Using this technique, GWs from two events, GW150914 and GW151226, were discovered in the first run of the Advanced LIGO detectors (September 2015 - January 2016). Previous attempts to measure GWs using laser interferometry started already in 2002 [10], but many improvements had to be made before the detectors were sensitive enough. That is because the amount of distance that the arms are stretched, is incredibly tiny (the strain is of the order 10^{-21}). It is also the reason why we have only detected GWs from sources with a very strong spacetime curvature thus far. Cosmic events that meet such requirements are binary systems, which we will discuss in the next chapter.

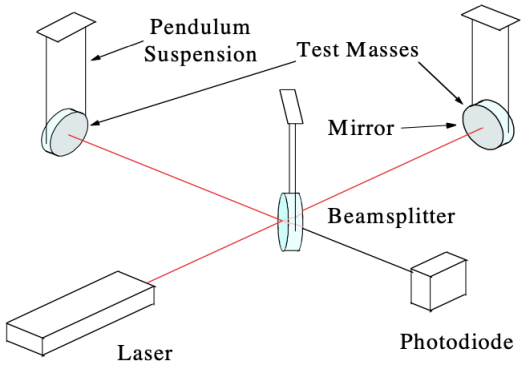

Figure 1: Schematic overview of a GW detector using laser interferometry. Taken from Pitkin et al. [9]

2 Gravitational waves from binary systems

As of today, all GW detections are from compact binary systems [11]. These systems consist of orbiting pairs of massive and dense objects such as black holes and neutron stars. They revolve around each other for millions of years and emit GWs while doing so. This stage in the existence of a binary is called the inspiral. As the GWs carry away orbital energy from the binary, the orbit decays into a closer orbit with a more rapidly changing quadrupole moment. Therefore stronger GWs are emitted and the orbit will decay even more. This cascade of events ends with the two objects coalescing, the so-called merger. Afterwards, there is one final stage called the ringdown. In this stage, the newly formed single black hole or neutron star undergoes some damped oscillations as a result from the merger.

The GWs that are detected thus far are from the late stages of inspiral, the merger and the ringdown. In these final phases of the binary's existence, the frequency and amplitude of the GWs are high enough to be detected by the interferometers [12]. Despite that, the signal only lasts for a short amount of time in the sensitive bandwidth of the detector, which is why signal-processing techniques like matched filtering (see e.g. [8]) are used to enhance the detectability of the signal.

In this chapter, we will first put the binary system in a mathematical framework in Section 2.1, then we will discuss the stationary phase approximation in Section 2.2 and finally we will consider a formalism that can help us model the dynamics of a binary in Section 2.3.

2.1 Signal from an inspiralling binary

In this thesis, we are going to investigate GW emission from binaries that are in the inspiral stage. To make the equations describing these GWs explicit, we will first define all the constituents of the binary.

Consider two point particles with masses, m_1 and m_2. The distance between both particles is defined as R and the distance from the binary to the observer is defined as r. The angle between the normal to the plane of the binary and the direction of the observer is defined as ι. Furthermore, we will assume that the masses are in a quasi-circular orbit around their common centre of mass with an orbital frequency ω. This assumption of quasi-circular orbits finds its validity in the equation for the time derivative of the eccentricity in binaries [13]. Due to a $(1-e^2)^{-5/2}$ term, the eccentricity decreases quickly over time through the emission of GWs, especially for highly eccentric orbits. In other words, the orbit circularizes fast and will be quasi-circular by the time the signal can be picked up by the detectors.

We place a Cartesian coordinate system in such a way that the centre of mass of the binary is at the origin, the observer is along the z-axis and the orbital plane crosses the x-axis. A schematic overview of this situation is made by Li [14] and depicted in Fig. 2.

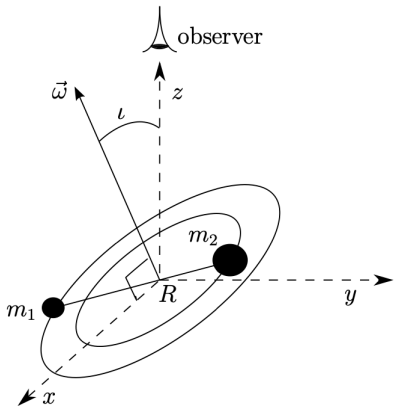

Figure 2: Schematic overview of a binary with masses m_1 and m_2 separated by a distance R. The center of mass is at the origin and the orbits are quasi-circular. The observer is along the z-axis and ω is the orbital frequency. The angle between the normal to the orbital plane and the observer is ι. Taken from Li [14].

In the situation just described, which is essentially a classic two-body problem, the position vector of both particles is given by [15]:

$$\begin{aligned}\vec{x}_1(t) &= \frac{m_2}{m_1+m_2} R\hat{\vec{e}}(t) = \frac{\mu}{m_1} R\hat{\vec{e}}(t),\\ \vec{x}_2(t) &= -\frac{m_1}{m_1+m_2} R\hat{\vec{e}}(t) = -\frac{\mu}{m_2} R\hat{\vec{e}}(t),\end{aligned} \tag{2.1}$$

where the reduced mass $\mu = m_1 m_2/(m_1+m_2)$ and the orientation vector $\hat{\vec{e}}(t)$ is given by the following expression:

$$\hat{\vec{e}}(t) = (\cos(\omega t), \cos(\iota)\sin(\omega t), \sin(\iota)\sin(\omega t)). \tag{2.2}$$

To determine the GW signal of the presumed binary, we have to look back at the mass quadrupole moment given by Eq. (1.12):

$$M^{k\ell}(t) = \frac{1}{c^2}\int d^3\vec{x}\, T^{00}(t,\vec{x}) x^k x^\ell = \int d^3\vec{x}\rho(t,\vec{x}) x^k x^\ell, \tag{2.3}$$

where we used $T^{00} = \rho c^2$. The density, ρ, in the case of two point particles is defined as:

$$\rho(t,\vec{x}) = m_1\delta^3(\vec{x} - \frac{\mu}{m_1} R\hat{\vec{e}}(t)) + m_2\delta^3(\vec{x} + \frac{\mu}{m_2} R\hat{\vec{e}}(t)). \tag{2.4}$$

Substituting Eq. (2.4) in Eq. (2.3), we can determine the mass quadrupole moment for the binary:

$$M^{k\ell}(t) = \left[m_1\frac{\mu^2}{m_1^2}R^2 + m_2\frac{\mu^2}{m_2^2}R^2\right]\hat{e}^k\hat{e}^\ell = \mu R^2\hat{e}^k\hat{e}^\ell. \tag{2.5}$$

Now we can make the expressions for h_+, Eq. (1.13), and $h_\times$, Eq. (1.14), explicit, including some arbitrary phase factor:

$$h_+ = \frac{4}{r}\frac{G\mu R^2\omega^2}{c^4}\frac{1+\cos^2(\iota)}{2}\cos\left(2\omega t_{\text{ret}} + 2\phi\right), \tag{2.6}$$

$$h_\times = \frac{4}{r}\frac{G\mu R^2\omega^2}{c^4}\cos\iota\sin\left(2\omega t_{\text{ret}} + 2\phi\right), \tag{2.7}$$

where we assumed that the orbital frequency and the distance between the two objects does not change much over a single orbit (adiabatic approximation), i.e. $\dot{\omega} = 0$ and $\dot{R} = 0$. Moreover, $t_{\text{ret}} = t - r/c$ is defined as the retarded time and comes from the dependence of $\ddot{M}^{k\ell}$ on this quantity (see Eq. (1.11)). We can clearly see from the two polarisation states that the binary radiates GWs at twice the orbital frequency.

Assuming that the two objects are far apart, we can set the centripetal and gravitational force equal and obtain:

$$\frac{m_1\left((\mu/m_1)R\right)^2\omega^2}{(\mu/m_1)R} = \frac{Gm_1m_2}{R^2}, \tag{2.8}$$

$$\omega^2 = GM/R^3, \tag{2.9}$$

which is in fact Kepler's third law [15]. We can use Eq. (2.9) to rewrite the expressions for the polarisation states in a more convenient form:

$$h_+ = \frac{4}{r}\frac{G\mathcal{M}_c^{5/3}\omega^{2/3}}{c^4}\frac{1+\cos^2\iota}{2}\cos\left(2\omega t_{\text{ret}} + 2\phi\right), \tag{2.10}$$

$$h_\times = \frac{4}{r}\frac{G\mathcal{M}_c^{5/3}\omega^{2/3}}{c^4}\cos\iota\sin\left(2\omega t_{\text{ret}} + 2\phi\right), \tag{2.11}$$

where we use the definition of the chirp mass:

$$\mathcal{M}_c = \frac{(m_1m_2)^{3/5}}{(m_1+m_2)^{1/5}}. \tag{2.12}$$

Now that we have written down the two polarisation states for the presumed binary, the question remains what the detector's response to the incoming GW looks like. For ground-based detectors, such as Advanced LIGO, often the so-called long-wavelength approximation is used to describe this response. In this approximation, it is assumed that the size of the detector is much smaller than the wavelength of the incoming GW and therefore the size of detector can be neglected. In reality, the phase of the GW changes slightly during the light-travel time of the laser beam in the detector [16]. In the long-wavelength approximation, the detector's response is just a projection of the strain in the GW-frame onto the detector [17] and can be written as [18]:

$$h(t) = F_+(\theta, \phi, \psi)\, h_+(t) + F_\times(\theta, \phi, \psi)\, h_\times(t), \tag{2.13}$$

where F_+ and $F_\times$ are written in terms of the spherical coordinates θ and ϕ and the polarization angle ψ. Collecting all the prefactors from Eq. (2.10) and Eq. (2.11) into a general time dependent amplitude $A(t)$, we can write the gravitational time domain waveform from a binary as:

$$h(t) = A(t)\sqrt{F_+^2\left(1+\cos^2(\iota)\right)^2 + F_\times^2 4\cos^2(\iota)}\, \cos\left(\Phi(t)+\varphi_0\right), \tag{2.14}$$

where we have rewritten $2\omega t_{\rm ret} + \phi$ as $\Phi(t)$ and φ_0 is defined as:

$$\varphi_0 = \arctan\left(\frac{-F_\times 2\cos(\iota)}{F_+\left(1+\cos^2(\iota)\right)}\right). \tag{2.15}$$

2.2 The stationary phase approximation

For the purpose of data analysis, it will be more convenient to work with a frequency domain waveform, $\tilde{h}(f)$, than with a time domain waveform, $h(t)$. This requires us to perform a Fourier transform on the time domain waveform found by the detector from Eq. (2.14). This calculation however, is computationally not feasible and difficult to perform analytically in its full form. That is why we will use an approximation, namely the stationary phase approximation.

Consider the lowest order waveform (Section 2.3 will explain about the different orders) from Eq. (2.14) in the time domain:

$$h(t) = QA(t)\cos\left(\Phi(t)+\phi_0\right), \tag{2.16}$$

where we define $Q = Q(\iota, \theta, \phi, \psi)$ as the square root from Eq. (2.14). To find the Fourier transform of Eq. (2.16), we need to perform the following integral:

$$\begin{aligned}\tilde{h}(f) &= Q\int_{-\infty}^{\infty} dt\, A(t)\cos\left(\Phi(t)+\phi_0\right)e^{2\pi i f t} \\ &= \frac{1}{2}Q\int_{-\infty}^{\infty} dt\, A(t)\left(e^{i[2\pi f t+(\Phi(t)+\phi_0)]} + e^{i[2\pi f t-(\Phi(t)+\phi_0)]}\right).\end{aligned} \tag{2.17}$$

The idea of the stationary phase approximation is to only evaluate the integral at the point of largest contribution $t = t_s$. When we look at the first term between the brackets, we can see $e^{i[2\pi f t+(\Phi(t)+\phi_0)]}$ as a unit vector in the complex plane where $2\pi f t + (\Phi(t)+\phi_0)$ is the angle with respect to the real axis. Due to the fact that the phase increases with time, this angle only grows. As a matter of fact, it grows quickly and what we have, is essentially a rapidly rotating vector whose integral effectively averages to zero. That means we can approximate Eq. (2.17) by:

$$\tilde{h}(f) \simeq \frac{1}{2}Q\int_{-\infty}^{\infty} dt\, A(t)e^{i(2\pi f t-(\Phi(t)+\phi_0))}. \tag{2.18}$$

The exponent we are left with does not have this effect, as there is now a minus term involved. In this case, the angle first grows and then becomes smaller, which indicates the existence of a stationary point where the contribution is the biggest. This observation yields us the following condition:

$$\frac{d}{dt}\left[2\pi f t - (\Phi(t)+\phi_0)\right]\Big|_{t=t_s} = 0, \tag{2.19}$$

$$2\pi f = \dot{\Phi}(t_s). \tag{2.20}$$

Next, we can expand the exponent of Eq. (2.18) around the stationary point:

$$2\pi ft - (\Phi(t) + \phi_0) = 2\pi ft_s - \Phi(t_s) - \phi_0 + 2\pi f(t - t_s) - \dot{\Phi}(t_s)(t - t_s) - \frac{1}{2}\ddot{\Phi}(t_s)(t - t_s)^2 + \dots \tag{2.21}$$

Because of the relation from Eq. (2.20), the fourth and fifth term on the right hand side of Eq. (2.21) cancel out and we are able to rewrite Eq. (2.18) as follows:

$$\tilde{h}(f) \simeq \frac{1}{2}Q \int_{-\infty}^{\infty} dt\, A(t) e^{i[2\pi f t_s - \Phi(t_s) - \phi_0 - \frac{1}{2}\ddot{\Phi}(t_s)(t-t_s)^2]}. \tag{2.22}$$

To further help us solve this integral, we use another approximation, namely that the amplitude varies slowly around t_s, which allows us to take it outside of the integral. Moreover, we define a new variable $x = \sqrt{\ddot{\Phi}(t_s)/2}\,(t - t_s)$. This yields:

$$\begin{aligned} \tilde{h}(f) &\approx \frac{1}{2}QA(t_s)e^{-i\phi_0}e^{i(2\pi f t_s - \Phi(t_s))} \int_{-\infty}^{\infty} dt\, e^{-\frac{i}{2}\ddot{\Phi}(t_s)(t-t_s)^2} \\ &\approx \frac{1}{2}QA(t_s)e^{-i\phi_0}e^{i(2\pi f t_s - \Phi(t_s))} \sqrt{\frac{2}{\ddot{\Phi}(t_s)}} \int_{-\infty}^{\infty} dx\, e^{-ix^2}. \end{aligned} \tag{2.23}$$

The integral that we are now left with, is a Gaussian integral with a standard solution:

$$\int_{-\infty}^{\infty} dx\, e^{-ix^2} = \sqrt{\pi} e^{-i\pi/4}. \tag{2.24}$$

Using this Gaussian, we can write down the final result of the frequency domain waveform:

$$\tilde{h}(f) = \frac{\sqrt{\pi}}{2} QA(t(f)) e^{-i\phi_0} \sqrt{\frac{2}{\ddot{\Phi}(t(f))}} e^{i\Psi(f)}, \tag{2.25}$$

where we used that at the stationary point $t = t(f)$ and where the phase is given by:

$$\Psi(f) = 2\pi f t(f) - \Phi(t(f)) - \frac{\pi}{4}. \tag{2.26}$$

One may wonder how accurate the stationary phase approximation exactly is. Studies on this [19, 20] have shown that especially for low-mass systems the approximation is very precise.

2.3 The post-Newtonian formalism

As already stated in Section 1.1, excluding some special cases, the EFE cannot be solved exactly. For that reason, approximation techniques are needed to gain full insight of the EFE. One such a approximation is described in Section 1.1. The post-Newtonian (PN) formalism describes an approximation which still has the Minkowski background spacetime with a small perturbation added to it, yet there is now an additional small parameter which is the characteristic orbital velocity v divided by the speed of light c [21]. When the inspiral of a binary is adiabatic, that is the time scale of the inspiral is much larger than the time scale of the orbit, the general relativistic equations of motion can be expanded in this small parameter v/c, where v is given by Kepler's third law:

$$v = (\pi G M f_{gw})^{1/3}, \tag{2.27}$$

where f_{gw} is the GW frequency (which is twice the orbital frequency, see Eq. (2.6)). In this expansion, Newtonian dynamics are recovered in the lowest order and general relativistic effects arise as higher order perturbations. The post-Newtonian formalism has been successful at describing the dynamics of a binary even at late stages of the inspiral [22]. Contrary to what might be expected at first sight, every additional power of v/c in the expansion corresponds to half a PN order extra, i.e. $(v/c)^3$ corresponds to 1.5PN.

As executed in Section 2.2, the stationary phase approximation can be used to Fourier transform the time domain waveform, which allowed us in the end to extract the phase as a function of the frequency. Starting with a higher order time domain waveform (3.5PN is the highest order to date [23]), the stationary phase approximation can also be applied, which is carried out in [24, 25]. This results in a Fourier transformed frequency domain waveform given by:

$$\tilde{h}(f) = \mathcal{A} f^{-7/6} e^{i\Psi(f)}, \tag{2.28}$$

where the amplitude $\mathcal{A} \propto \mathcal{M}_c^{5/6} Q(\text{angles})/r$, and $\Psi(f)$ is the phase up to 3.5PN given by:

$$\Psi(f) = 2\pi f t_c - \phi_c - \frac{\pi}{4} + \frac{3}{128\eta \left(\frac{v}{c}\right)^5} \sum_{k=0}^{7} \phi_k \left(\frac{v}{c}\right)^k, \tag{2.29}$$

where $\eta = m_1 m_2/(m_1+m_2)^2$ is the dimensionless mass ratio, t_c and ϕ_c are respectively the time and phase of coalescence and the coefficients ϕ_k in the Fourier phase are given in [22]. In principle, this expansion has infinite terms, but this is how many coefficients have been calculated currently.

In this thesis, we will be using the GW phase in the PN approximation. The presence of electric charges in a binary will influence this phase and allow us to extract an additional PN order in Section 4.3. In the upcoming chapter, we will first discuss whether the presence of electric charges is a realistic possibility for black holes.

3 Black holes and electric charge

According to the no-hair theorem, it is possible to completely characterize any black hole (BH) by three and only three classical, externally observable parameters: its mass (M), its angular momentum (J) and its electric charge (Q) [26]. All other information about a BH is hidden inside its event horizon, unreachable for outside observers. A lot of time and research is spent on figuring out the mass and angular momentum of a BH, however the third parameter, electric charge, is often neglected and therefore poorly constrained [27]. Usually the motivation behind this is the assumption that if a BH has any net electric charge, it will quickly discharge because of the presence of a plasma around the BH. In this chapter, we will first discuss the different metric possibilities for a BH (Section 3.1). Second, we will motivate how a BH may possess a net electric charge and how it could acquire a steady flow of electric charges (Section 3.2). Finally, we will discuss the consequences of a charged BH (Section 3.3).

3.1 Different metrics

There are four different metrics that correspond to BH solutions in GR [28]. The different solutions are named after the physicist(s) that discovered them. The first and most straightforward one is the Schwarzschild BH, where the Schwarzschild metric is a solution to GR of a point particle without angular momentum nor electric charge. A second solution is the Kerr metric, which is the spinning version of the Schwarzschild metric. The two solutions that include electric charge are the Reissner-Nordström metric and the Kerr-Newman metric. The former is a BH which has no angular momentum, but does have electric charge, whilst the latter is a generalization of the Reissner-Nordström metric with both angular momentum as well as electric charge.

Most BHs are expected to follow the Kerr metric, as electric charge is neglected and most stars have angular momentum which they cannot get rid off during their collapse into a BH due to conservation of angular momentum. For an extremal BH [29], there is a so-called extremal charge, which is the maximum amount of charge a BH can possess. This relation is given by [27]:

$$Q_{\text{extremal}} = 2M\sqrt{\pi\epsilon_0 G\,(1-\tilde{a}^2)}, \tag{3.1}$$

where M is the mass of the BH and $\tilde{a}$ is the dimensionless spin. For the non-rotating Reissner-Nordström metric, $\tilde{a} = 0$, this results in an extremal charge of

$$Q_{\text{extremal}} = 2\sqrt{\pi\epsilon_0 G}M = 1.7\times10^{20}\left(\frac{M}{M_\odot}\right)C, \tag{3.2}$$

where $M_\odot$ is the mass of the sun. As we will be dealing with a dimensionless charge-to-mass ratio later on, it is convenient to rewrite Eq. (3.2) as:

$$\frac{1}{\sqrt{\epsilon_0 G}}\frac{Q_{\text{extremal}}}{M} = 2\sqrt{\pi} \approx 3.54491. \tag{3.3}$$

This is of course only a theoretical limit, but it does provide us with a first upper bound and an insight on the values that can possibly be obtained. In the next section, we will discuss some realistic mechanisms that can provide a BH with electric charge.

3.2 How can black holes acquire charge?

Although in most research electric charge is considered negligible, during the last couple of years this assumption has been revisited due to the anticipated discovery of a BH-neutron star binary through GW observations [30–32].

A first mechanism that provides BHs with electric charge was derived by Bally and Harrison in 1978 [33] who generalised a principle discovered by Eddington in 1926 [34]. He explained how stars should have a small positive charge to prohibit protons and electrons in the stellar atmosphere from further separation, as

protons are gravitationally stronger bound to a star due to a mass difference by a factor of almost 2000. Bally and Harrison showed that any macroscopic body in the Universe is positively charged with a charge-to-mass ratio of about 100 Coulomb per solar mass. As an example, this mechanism would constrain the charge of the super massive BH in the center of our galaxy, Sgr A^* ($M = 4 \times 10^6 M_\odot$ [35]), at $\sim 10^8 C$. For those shocked on their beliefs of a electrically neutral universe: that is still true. The net positive charges of these macroscopic bodies is compensated by a negatively charged, freely expanding intergalactic medium [36].

Another, perhaps more interesting mechanism that could provide a BH with a steady flow of charged particles is the Wald charge derived by Wald in 1974 [37]. He showed that a rotating BH immersed in a uniform magnetic field induces electric charges. Essentialy, it can be seen as a form of Faraday induction on a huge scale, where the rotation of the BH in the magnetic field gives rise to an electric potential and therefore an electric field. The electric potential is set between infinity and the BH horizon and it causes the selective accretion of charged particles from the plasma around the BH (only positive or only negative depending on the alignment of the rotation axis of the BH). The potential difference looks as follows (in geometric units) [27]:

$$\Delta\phi = \phi_H - \phi_\infty = \frac{Q - 2aMB_0}{2M}, \tag{3.4}$$

where $a = (Jc)/(GM)$ is the spin parameter ($a = J/M$ in geometric units) and B_0 is the external magnetic field. We can clearly see that the accretion of charged particles continues until some equilibrium value:

$$Q_w = 2aMB_0, \tag{3.5}$$

where Q_w is the induced electric charge through the Wald mechanism. Using the fact that for a Kerr BH $J = Ma \leq M^2$ [37], the charge-to-mass ratio of a BH due to the Wald charge has an upper bound:

$$\frac{Q_w}{M} = 2B_0 \left(\frac{J}{M}\right) \leq 2B_0 M, \tag{3.6}$$

$$\frac{1}{\sqrt{\epsilon_0 G}} \frac{Q_w}{M} \leq 2.4 \times 10^{-5} \left(\frac{B_0}{10^{15} G}\right) \left(\frac{M}{M_\odot}\right), \tag{3.7}$$

where in the second expression, the geometric units are converted back to units of Gauss and solar mass and we introduced a factor $1/\sqrt{\epsilon_0 G}$ to create a dimensionless charge-to-mass ratio. Furthermore, we can use the conditions for a Kerr BH as the induced charge will be small enough not to distort the Kerr spacetime metric [27, 38, 39].

The question that we must ask ourselves is whether the assumption of BHs immersed in a magnetic field is reasonable and whether the magnetic field is big enough to have any real impact on the charge-to-mass ratio. There are a couple of possible ways in which a magnetic field could be present. Perhaps the most straightforward way is when a strongly magnetised neutron star is in the vicinity of a BH. This has been investigated by e.g. [31, 32]. In the absence of a neutron star, there is research on how accretion disks could be magnetised [40, 41], additionally numerical simulations have shown that accretion disks can support magnetic fields up to $10^{15} G$ [42]. Moreover, something we can directly observe is the Blandford-Znajek mechanism [43]. In this process, the magnetic field lines around a BH are dragged along with its rotation. These rotating field lines induce an electromagnetic force that accelerates charged particles at relativistic speeds along the axis of rotation which is called a relativistic jet. In essence, this is a form of magnetic braking where rotational energy from the BH is extracted and therefore the BH rotation slows down. The characteristic time scales we observe with the Blandford-Znajek process [42] show us that there should be magnetic fields present of up to 10^{15} G.

This magnetic field condition alongside the fact that any BH is generally rotating, show that a stable non-zero charge of a BH is credible. The BH will favour accreting charges energetically until the equilibrium value is reached, instead of immediately discharge. In the next section, we will discuss the consequences that this brings along.

3.3 Consequences of a charged black hole

As mentioned, the electric charge of a BH will probably not be large enough to distort the spacetime metric of a Kerr BH. That does not mean electric charge is irrelevant, given that there are many processes which will be influenced by a BH that possesses electric charge. We will cover one of them in detail in this section.

For any massive object, there is a so-called innermost stable circular orbit (ISCO) which is the smallest circular orbit in which a test particle can stably orbit that object. Due to a charged BH the ISCO is shifted for neutral and charged matter. In Zajaček et al. [27], this effect has been investigated for the super massive BH Sgr A*. For an uncharged, non-spinning Schwarzschild metric, the ISCO is located at $r_{ISCO} = 3r_s$, where $r_s = 2GM/c^2$ is the Schwarzschild radius [44]. When the super massive BH is positively or negatively charged, the ISCO for positive or negative test particles will shift as shown in Fig. 3. We see that already for a small charge of $10^3 C$, the ISCO starts to move. At the low ends, the ISCO can shift to $1.83r_s$. This can be of importance when e.g. determining the spin of a BH through the position of the ISCO, as a r_{ISCO} of $1.83r_s$ due to electric charge, could also be caused by a non-charged BH with a prograde spin of $a = 0.64$. The presence of a magnetic field would shift the ISCO even more [45], which means these two effects together cause uncertainty on the spin determination of a BH by looking at the ISCO.

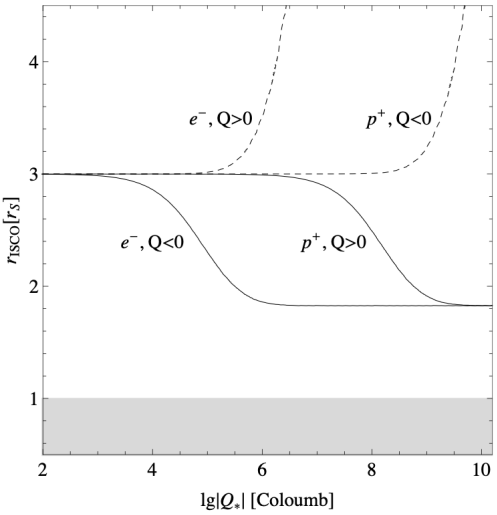

Figure 3: The radius of the ISCO r_s (in Schwarzschild radii) as function of the electric charge Q (in Coulomb) for four different cases: positively or negatively charged test particles (electrons or protons) orbiting the positively or negatively charged super massive BH Sgr A*. Taken from Zajaček et al. [27].

In literature, more effects can be found that are influenced by BHs possessing some net electric charge, like charged BHs being sources of ultra high energy cosmic rays [46] or spinning charged BHs creating their own magnetic dipole to power a BH pulsar [30]. The importance of electric charge may even be greater in unknown or poorly understood mechanisms in the Universe. Eq. (3.7) shows that under certain circumstances, the charge-to-mass ratio can build up to significant values. A way to set upper bounds on electric charges is through GW analysis. In the upcoming chapters, we will first investigate in which way electric charges will modify the gravitational waveform and subsequently we will use data from GW events to set bounds.

4 Effect of charges on the gravitational waveform

The compact binary systems we are going to study, will be structured as described in Section 2.1. The only difference is that we introduce the presence of electric charge here by assuming that masses m_1 and m_2 have an electric charge of respectively q_1 and q_2. The main effect of these charges on the orbital motion and hence the GW signal can be calculated by solving the energy balance equation to leading order in small quantities. The energy balance equation for compact binaries in the inspiral stage, which fall under the PN approximation, is given in the form [23]:

$$\frac{dE}{dt} = -\mathcal{P}, \tag{4.1}$$

where E is the total energy of the binary and $\mathcal{P}$ is the total power (energy per unit time) radiated by the binary. In this energy balance equation, it is assumed that the orbits are circular and the energy is globally conserved. Specifically, the energy radiated away is equal to loss of energy of the circular orbit [47].

In this chapter, we will first calculate the total energy of the binary (Section 4.1), then the total radiated power (Section 4.2) and finally we will determine what the altered gravitational waveform looks like (Section 4.3).

4.1 Energy

The left-hand side of Eq. (4.1) requires us to calculate the total energy of the binary. Normally, the energy would just be the orbital energy of the system, however the presence of electric charges means that we also have to deal with dipole energy. We can set up the following action for a compact binary system [7], where we include an additional term for the Coulomb interaction between the two point charges separated by a distance R [48]:

$$S = \int dt \left[\frac{\mu}{R}(\dot{R}^2 + R^2\dot{\phi}^2) + \frac{G\mu M}{R} - \frac{1}{4\pi\epsilon_0}\frac{q_1 q_2}{R} \right], \tag{4.2}$$

where μ is the reduced mass as defined before, $M = m_1 + m_2$ is the total mass of the binary and ϵ_0 is the electric permittivity of the vacuum. In this action integral we can clearly both see the gravitational and electromagnetic interaction between the two bodies. From Eq. (4.2) we can extract the Lagrangian:

$$L = \frac{\mu}{2}(\dot{R}^2 + R^2\omega^2) + \frac{G\mu M}{R}(1+\lambda), \tag{4.3}$$

where we define $\lambda = -\frac{1}{4\pi\epsilon_0 G}\frac{q_1 q_2}{\mu M}$ as our dimensionless small variable and we set the time derivative of the phase, $\dot{\phi}$, equal to the orbital frequency, ω. By assuming an adiabatic approximation (which is valid in the inspiral), we can neglect $\dot{R}$ and use the Euler-Lagrange equations [15] on Eq. (4.3) to obtain an equation of motion:

$$\frac{\partial L}{\partial R} - \frac{d}{dt}\frac{\partial L}{\partial \dot{R}} = 0, \tag{4.4}$$

$$\mu R^3\omega^2 = G\mu M(1+\lambda). \tag{4.5}$$

We can try to solve this now for R, but let us first have a look at what the solution would be without electric charges. In the case of two point particles orbiting in circular motion, the motion would be governed by Kepler's third law (see Eq. (2.9)):

$$R_0(\omega) = (GM)^{1/3}\omega^{-2/3}. \tag{4.6}$$

As we assume that the electric charges only have a small effect on the motion, i.e. $dE_{dip}/dt \ll dE_{orb}/dt$, we can write Eq. (4.6) with a small perturbation added to it:

$$R(\omega) = R_0(\omega)(1 + \delta R(\omega)). \tag{4.7}$$

Substituting Eq. (4.7) into Eq. (4.5) and writing out Kepler's law from Eq. (4.6) yields:

$$\begin{aligned} \mu GM\omega^{-2}(1+\delta R(\omega))^3\omega^2 &= G\mu M(1+\lambda), \\ (1+\delta R(\omega))^3 &= 1+\lambda. \end{aligned} \tag{4.8}$$

Expanding this expression and neglecting terms of δR^2 and higher, allows us to solve for $\delta R(\omega)$:

$$\begin{aligned} 1 + 3\,\delta R(\omega) &\approx 1 + \lambda, \\ \delta R(\omega) &\approx \frac{1}{3}\lambda. \end{aligned} \tag{4.9}$$

This means we end up with the following perturbed Kepler's third law in the case with electric charges:

$$R(\omega) = (GM)^{1/3}\omega^{-2/3}(1 + \frac{1}{3}\lambda). \tag{4.10}$$

As our Lagrangian is explicitly independent of time, we obtain the following expression for the energy [15]:

$$\begin{aligned} E &= \left(\sum_{i=1}^{N} \frac{\partial L}{\partial \dot{q}_i}\dot{q}_i\right) - L \\ &= \frac{\mu}{2}R^2\omega^2 - \frac{G\mu M}{R}(1 + \lambda). \end{aligned} \tag{4.11}$$

To express the energy only in terms of the orbital frequency (which will be convenient later on), we fill the perturbed Kepler law from Eq. (4.10) into Eq. (4.11), expand in small quantities and thereafter neglect terms of λ^2 and higher. We then obtain the following term for the energy:

$$\begin{aligned} E(\omega) &\approx \frac{\mu}{2}(GM\omega)^{2/3}(1 + \frac{1}{3}\lambda)^2 - \mu(GM\omega)^{2/3}(1 + \lambda)(1 - \frac{1}{3}\lambda) \\ &\approx -\frac{1}{2}\mu(GM\omega)^{2/3}(1 + \frac{2}{3}\lambda). \end{aligned} \tag{4.12}$$

4.2 Radiated power

Now that we have found the energy of the binary system, we have to determine the power radiated by the binary which consists of two parts. There is the gravitational radiation and the electromagnetic radiation. For both we take the first non-zero multipole term, which means - in GR - gravitational quadrupole radiation, $\mathcal{P}_{GW}$, and electromagnetic dipole radiation, $\mathcal{P}_{em}$. The former is equal to the GW energy per unit time from Eq. (1.9):

$$\mathcal{P}_{GW} = \frac{dE_{GW}}{dt} = \frac{c^3 r^2}{16\pi G}\int_{\mathcal{S}} d\Omega \left\langle \dot{h}_+^2 + \dot{h}_\times^2 \right\rangle. \tag{4.13}$$

In the absence of electric charges this yields the following [7]:

$$\frac{dE_{GW}}{dt} = \frac{32}{5}\frac{G^{7/3}}{c^5}(\mathcal{M}_c\omega)^{10/3}, \tag{4.14}$$

where the definition of the chirp mass from Eq. (2.12) is used. To make this equation compatible for our case, we have to make an adjustment. In the expressions for h_+ and $h_\times$ from respectively Eq (2.6) and Eq. (2.7), we see a R^2 term. Due to the perturbed Kepler law from Eq. (4.10), this introduces a $(1 + \frac{1}{3}\lambda)^2$ correction to both polarisation states. In Eq. (4.13), the derivatives of h_+ and $h_\times$ are both squared, which means that the correction is also squared and we get an extra factor $(1 + \frac{1}{3}\lambda)^4$ in our expression for $\mathcal{P}_{GW}$. Writing out the full expressions for h_+ and $h_\times$ and performing the integral from Eq. (4.13) will show that this is the only correction we need to make. We end up with the following term for the gravitational radiation:

$$\mathcal{P}_{GW} = \frac{dE_{GW}}{dt} = \frac{32}{5}\frac{G^{7/3}}{c^5}(\mathcal{M}_c\omega)^{10/3}(1 + \frac{1}{3}\lambda)^4 \approx \frac{32}{5}\frac{G^{7/3}}{c^5}(\mathcal{M}_c\omega)^{10/3}(1 + \frac{4}{3}\lambda), \tag{4.15}$$

where once again we neglected terms of λ^2 and higher.

Next, we are going to derive what the second part of the radiated power is. To calculate the electromagnetic dipole radiation, which is the power emitted by the electromagnetic waves, we need to compute the

electric and magnetic field. We are going to use the far-field approximation, in which the general expressions look as follows [49]:

$$\vec{E}(\vec{r},t) \simeq -\frac{1}{4\pi\epsilon_0}\frac{1}{c^2 r}\frac{\partial}{\partial t}\int \vec{j}_\perp dV', \tag{4.16}$$

$$\vec{B}(\vec{r},t) \simeq \frac{1}{4\pi\epsilon_0}\frac{1}{c^3 r^2}\frac{\partial}{\partial t}\left[\int \vec{j}_\perp dV'\right] \times \vec{r}, \tag{4.17}$$

where r is the distance from the observer to the source and we define $\vec{j}$, the current distribution, in the point particle limit as follows:

$$\vec{j} = \rho\vec{v} = q_1\delta^3(\vec{x}-\vec{x_1})\vec{v} + q_2\delta^3(\vec{x}-\vec{x_2})\vec{v}. \tag{4.18}$$

Using $\vec{j}$ and the position vectors from Eq. (2.1), we can fill in Eq. (4.16) and deduce the electric field.

$$\begin{aligned}\vec{E}(\vec{r},t) &\simeq -\frac{1}{4\pi\epsilon_0}\frac{1}{c^2 r}(q_1\ddot{\vec{x}}_{1\perp} + q_2\ddot{\vec{x}}_{2\perp}) \\ &= -\frac{1}{4\pi\epsilon_0}\frac{1}{c^2 r}\left(q_1\frac{\mu}{m_1}R\ddot{\hat{\vec{e}}}_\perp(t) - q_2\frac{\mu}{m_2}R\ddot{\hat{\vec{e}}}_\perp(t)\right) \\ &= \frac{1}{4\pi\epsilon_0}\frac{\mu R\omega^2}{c^2 r}\left(\frac{q_1}{m_1}-\frac{q_2}{m_2}\right)\begin{pmatrix}\cos(\omega t)\\ \cos(\iota)\sin(\omega t)\\ 0\end{pmatrix}.\end{aligned} \tag{4.19}$$

The calculation to obtain the magnetic field is almost analogous, the only difference is the cross product with r in the direction perpendicular to the electric field.

$$\begin{aligned}\vec{B}(\vec{r},t) &\simeq -\frac{1}{4\pi\epsilon_0}\frac{\mu R\omega^2}{c^3 r^2}\left(\frac{q_1}{m_1}-\frac{q_2}{m_2}\right)\begin{pmatrix}\cos(\omega t)\\ \cos(\iota)\sin(\omega t)\\ 0\end{pmatrix}\times\begin{pmatrix}0\\0\\r\end{pmatrix} \\ &= -\frac{1}{4\pi\epsilon_0}\frac{\mu R\omega^2}{c^3 r}\left(\frac{q_1}{m_1}-\frac{q_2}{m_2}\right)\begin{pmatrix}\cos(\iota)\sin(\omega t)\\ -\cos(\omega t)\\ 0\end{pmatrix}.\end{aligned} \tag{4.20}$$

Now that we have derived the electric and the magnetic field, we can calculate the Poynting vector which describes the energy flux density (energy per unit area, per unit time) of an electromagnetic wave [48]:

$$\vec{S} = \frac{1}{\mu_0}\vec{E}\times\vec{B}, \tag{4.21}$$

where μ_0 is the vacuum permeability. Filling Eq. (4.19) and Eq. (4.20) into the definition of the Poynting vector yields:

$$\vec{S} = -\frac{1}{\mu_0}\frac{1}{(4\pi\epsilon_0)^2}\frac{\mu^2 R^2\omega^4}{c^5 r^2}\left(\frac{q_1}{m_1}-\frac{q_2}{m_2}\right)^2\begin{pmatrix}0\\0\\-\cos^2(\omega t)-\cos^2(\iota)\sin^2(\omega t)\end{pmatrix}. \tag{4.22}$$

At this point we introduce a dimensionless variable which includes a relative charge difference. It is defined as follows:

$$\xi^2 = \frac{1}{4\pi\epsilon_0 G}\left(\frac{q_1}{m_1}-\frac{q_2}{m_2}\right)^2. \tag{4.23}$$

This allows us to write the Poynting vector as:

$$\vec{S} = \frac{1}{\mu_0}\frac{1}{4\pi\epsilon_0}\frac{G\mu^2 R^2\omega^4}{c^5 r^2}\xi^2\begin{pmatrix}0\\0\\\cos^2(\omega t)+\cos^2(\iota)\sin^2(\omega t)\end{pmatrix}. \tag{4.24}$$

In order to calculate the radiated power, we need to perform two more steps. First, we integrate over any closed surface surrounding the dipole:

$$\begin{aligned} P &= \int \mid \vec{S} \mid d\vec{a} = \int r^2 \sin(\iota) d\iota d\phi \mid \vec{S} \mid \\ &= 2\pi \frac{c^2 \epsilon_0}{4\pi\epsilon_0} \frac{G\mu^2 R^2 \omega^4}{c^5} \xi^2 \int_0^\pi \left[\cos^2(\omega t) + \cos^2(\iota)\sin^2(\omega t)\right] \sin(\iota) d\iota \\ &= \frac{1}{2} \frac{G\mu^2 R^2 \omega^4}{c^3} \xi^2 \left[2\cos^2(\omega t) + \frac{2}{3}\sin^2(\omega t)\right], \end{aligned} \tag{4.25}$$

where we used the relation $c = 1/\sqrt{\epsilon_0 \mu_0}$. Second, we take a time average of one period over Eq. (4.25) as that is a quantity that is independent of short-term fluctuations:

$$\begin{aligned} \mathcal{P}_{em} = \langle P \rangle &= \frac{1}{2} \frac{G\mu^2 R^2 \omega^4}{c^3} \xi^2 \left\langle 2\cos^2(\omega t) + \frac{2}{3}\sin^2(\omega t) \right\rangle \\ &= \frac{2}{3} \frac{G\mu^2 R^2 \omega^4}{c^3} \xi^2. \end{aligned} \tag{4.26}$$

Using the perturbed Kepler law from Eq. (4.10), we can expand this to leading order and rewrite it into a more convenient expression:

$$\begin{aligned} \mathcal{P}_{em} &= \frac{2}{3} \frac{G\mu^2 \left[(GM)^{2/3} \omega^{-4/3} \left(1 + \frac{1}{3}\lambda\right)^2\right] \omega^4}{c^3} \xi^2 \\ &\approx \frac{2}{3} \frac{G^{5/3} \mu \mathcal{M}_c^{5/3} \omega^{8/3}}{c^3} \xi^2 \left(1 + \frac{2}{3}\lambda\right). \end{aligned} \tag{4.27}$$

To summarize, we have found that the total radiated power sent out by the binary is composed of two parts, the gravitational radiation from Eq. (4.13) and the electromagnetic radiation from Eq. (4.27). Added up, this yields:

$$\mathcal{P} = \mathcal{P}_{GW} + \mathcal{P}_{em} = \frac{32}{5} \frac{G^{7/3}}{c^5} (\mathcal{M}_c \omega)^{10/3} (1 + \frac{4}{3}\lambda) + \frac{2}{3} \frac{G^{5/3} \mu \mathcal{M}_c^{5/3} \omega^{8/3}}{c^3} \xi^2 (1 + \frac{2}{3}\lambda). \tag{4.28}$$

Through a redefinition of the chirp mass, we can absorb the λ terms. By setting $\mathcal{M}_c^{5/3} \to \tilde{\mathcal{M}}_c^{5/3} \equiv \mathcal{M}_c^{5/3}(1 + (2/3)\lambda)$, both in the gravitational and electromagnetic power the λ terms are absorbed in the chirp mass. As the reduced mass μ is an independent observable from the chirp mass, we do not have the shift μ as well. This redefinition does mean that the observed value for the chirp mass differs from the intrisic value. However, measuring the correct value for the chirp mass is not of our interest [2]. Using this redefinition, we can write the total radiated power as:

$$\mathcal{P} = \mathcal{P}_{GW} + \mathcal{P}_{em} = \frac{32}{5} \frac{G^{7/3}}{c^5} (\tilde{\mathcal{M}}_c \omega)^{10/3} + \frac{2}{3} \frac{G^{5/3} \mu \tilde{\mathcal{M}}_c^{5/3} \omega^{8/3}}{c^3} \xi^2. \tag{4.29}$$

As we assume that the dipolar electromagnetic radiation is small compared to the quadrupolar GW radiation, i.e. $\mathcal{P}_{em} \ll \mathcal{P}_{GW}$, we can write the total power from Eq. (4.29) as the GW radiation with a small correction added to it, which will be the necessary form for the total power in Section 4.3.

$$\mathcal{P} = \mathcal{P}_{GW}(1 + \kappa \omega^{-2/3}), \tag{4.30}$$

where we define the small variable κ as follows:

$$\kappa = \frac{5}{48} G^{-2/3} c^2 \mu \tilde{\mathcal{M}}_c^{-5/3} \xi^2. \tag{4.31}$$

[2] Note that neglecting charge effects leads to an overestimation of the measured chirp mass which could be taken into consideration in other research.

4.3 Leading order modifications of the waveform phase

In essence, we are now able to fill in Eq. (4.1) and find the GW phase by integrating over the orbital frequency. However, the resulting integral cannot be solved analytically. To circumvent this problem, a different angle will be taken. The derivative of the GW phase with respect of the frequency yields:

$$\begin{aligned}\frac{d\Psi}{df} &= 2\pi t(f) + 2\pi f t'(f) - \dot{\Phi} t'(f) \\ &= 2\pi t(f) + t'(f)[2\pi f - \dot{\Phi}] = 2\pi t(f),\end{aligned} \tag{4.32}$$

where the prime denotes the derivative to the frequency and the term between the brackets is equal to zero because of Eq. (2.20). Differentiating again, the second derivative of the phase can be written in terms of a first derivative of the energy and the power:

$$\frac{d^2\Psi}{df^2} = 2\pi \frac{dt}{df} = 2\pi \frac{dt}{dE}\frac{dE}{df} = 2\pi \frac{dE/df}{dE/dt} = -2\pi \frac{dE/df}{\mathcal{P}}, \tag{4.33}$$

where we used Eq. (4.1). As the energy and the power are written in terms of the orbital frequency, we use the relation $\omega = \pi f$ to rewrite Eq. (4.33):

$$\frac{d^2\Psi}{d\omega^2} = -2\frac{dE/d\omega}{\mathcal{P}}. \tag{4.34}$$

For the numerator of Eq. (4.34), we take the derivative of Eq. (4.12) with respect to ω:

$$\begin{aligned}\frac{dE}{d\omega} &= -\frac{1}{3}\mu (GM)^{2/3}\omega^{-1/3}(1 + \frac{2}{3}\lambda) \\ &= -\frac{1}{3}G^{2/3}\tilde{\mathcal{M}}_c{}^{5/3}\omega^{-1/3},\end{aligned} \tag{4.35}$$

where we used the redefinition of the chirp mass. We can now take advantage of writing the power as in Eq. (4.30), since it allows us to write Eq. (4.34) in a form which is analytically integrable. Substituting Eq. (4.35) and Eq. (4.30) into Eq. (4.34) and expanding in small quantities yields:

$$\begin{aligned}\frac{d^2\Psi}{d\omega^2} &= -2\frac{-\frac{1}{3}G^{2/3}\tilde{\mathcal{M}}_c{}^{5/3}\omega^{-1/3}}{\mathcal{P}_{GW}(1+\kappa\omega^{-2/3})} \approx \frac{\frac{2}{3}G^{2/3}\tilde{\mathcal{M}}_c^{5/3}\omega^{-1/3}(1-\kappa\omega^{-2/3})}{\frac{32}{5}\frac{G^{7/3}}{c^5}(\tilde{\mathcal{M}}_c\omega)^{10/3}} \\ &\approx \frac{5}{48}(G\tilde{\mathcal{M}}_c)^{-5/3}c^5\omega^{-11/3}(1-\kappa\omega^{-2/3}) = \frac{5}{48}(G\tilde{\mathcal{M}}_c)^{-5/3}c^5\omega^{-11/3} - \frac{5}{48}(G\tilde{\mathcal{M}}_c)^{-5/3}c^5\kappa\omega^{-13/3},\end{aligned} \tag{4.36}$$

where we used Eq. (4.15) in the second step. Integrating this expression twice gives us the modified waveform phase up to leading order in small quantities:

$$\begin{aligned}\Psi(\omega) &= \frac{3}{128}(G\tilde{\mathcal{M}}_c)^{-5/3}c^5\omega^{-5/3} - \frac{3}{224}(G\tilde{\mathcal{M}}_c)^{-5/3}c^5\kappa\omega^{-7/3} + C_1\omega + C_2 \\ &= \frac{3}{128}(G\tilde{\mathcal{M}}_c)^{-5/3}c^5\omega^{-5/3} - \frac{3}{128}\frac{5}{84}G^{-7/3}\mu\tilde{\mathcal{M}}_c^{-10/3}c^7\xi^2\omega^{-7/3} + C_1\omega + C_2,\end{aligned} \tag{4.37}$$

where C_1 and C_2 are constants of integration and we have written out κ with Eq. (4.31).

Since the waveform in the inspiral is modelled in the PN approximation, we rewrite the newly found phase to the form of Eq. (2.29).

$$\Psi(\omega) = \frac{3}{128}(G\tilde{M}\omega)^{-5/3}\frac{M^2}{m_1m_2}c^5 - \frac{3}{128}\frac{5}{84}(G\tilde{M}\omega)^{-7/3}\frac{M^2}{m_1m_2}c^7\xi^2 + C_1\omega + C_2, \tag{4.38}$$

$$\Psi(\omega) = \frac{3}{128\eta\left(\frac{\tilde{v}}{c}\right)^5} - \frac{3}{128\eta\left(\frac{\tilde{v}}{c}\right)^7}\frac{5}{84}\xi^2 + 2\omega t_c - \phi_c - \frac{\pi}{4}, \tag{4.39}$$

where we used the dimensionless mass ratio η, the non-perturbed orbital velocity from Eq. (2.27) and the fact that a redefinition of the chirp mass equals a redefinition of the total mass because of $\mathcal{M}_c = M\eta^{3/5}$. Furthermore, comparing with the PN approximation, we gave the constants of integration a value where $C_1 = 2t_c$ and $C_2 = -\phi_c - \pi/4$.

Using the relation $\omega = \pi f$, we can compare Eq. (4.39) with Eq. (2.29) and one thing immediately stands out: there is an additional term that goes like $(v/c)^{-7}$. This is due to the electromagnetic dipolar emission and named as the -1PN term [3]. The corresponding coefficient is given by:

$$\phi_{-2} = -\frac{5}{84}\xi^2 = -\frac{5}{84}\frac{1}{4\pi\epsilon_0 G}\left(\frac{q_1}{m_1} - \frac{q_2}{m_2}\right)^2 \leq 0. \tag{4.40}$$

We arrive here at the important result that in the case of electric charges in a binary, the coefficient of the -1PN term, ϕ_{-2}, can only take on non-positive values.

One may wonder why we only end up with the -1PN and 0PN terms in the phase. This has to do with the fact that we only include the quadrupole radiation and not higher multipole terms along with the fact that we only deal with h up to leading order. In the data analysis from Chapter 5, we will reinstate the higher PN orders. However, as we expect ξ^2 to be small, we will only take into account the gravitational effects of the higher PN orders and consider the electromagnetic effects just from leading order.

In the upcoming chapter, we will use the newly found relation from Eq. (4.40) to obtain bounds on the relative charge difference of actual GW events.

[3] The sum from Eq. (2.29) is extended to start with $k = -2$.

5 Application to selected GW signals from binary black holes

Using data from experimental observations of five binary BH GW events (GW150914, GW151226, GW170104, GW170608, GW170814), Abbott et al. [50] derive 90% credible intervals on the corresponding coefficient of the -1PN term. Their aim was to see how consistent the data from these observations are with the predictions from GR. As described in [50], deviations from GR result in relative shifts of the waveform coefficients, which for the inspiral parameters look like: $\phi_i \to (1 + \delta\phi_i)\phi_i$, where $\delta\phi_i$ is the relative shift and i denotes the powers in v/c beyond leading order (where the leading order term is now $(v/c)^{-7}$). Given that -1PN term is absent in the GR phasing, the relative shift turns into an absolute deviation, i.e. $\delta\phi_{-2} = \phi_{-2}$. To test this parameter, they treat it as an additional, free parameter in the waveform model.

We are going to perform a statistical test that is comparable to the one carried out in [50], with one essential difference. As derived in Section 4.3, the presence of a net electric charge in a BH binary induces a -1PN term in the phase, $\delta\phi_{-2}$, that can only be non-positive. Therefore, when we ask ourselves whether we can bound the charge, and thus the -1PN term, we can constrain a priori $\delta\phi_{-2}$ to non-positive values only. This chapter will describe the consequences of using this restriction on the sign of $\delta\phi_{-2}$. We analyze the same binary BH events as in [50] due to their good signal in the inspiral regime.

In Section 5.1, we will discuss how the data analysis for GW events exactly works, i.e. how does the incoming data from the detector get translated into useful information about the binary BH. In Section 5.2, we will address a computational tool that will help us with the data-analysis. Finally, in Section 5.3, we will present the resulting bounds.

5.1 Parameter estimation

The basic goal of GW data analysis is to deduce, as accurately as possible, the real value of some parameter, given the observed data. This is commonly called parameter estimation and for a compact binary BH system, there is a multi-dimensional parameter called $\vec{\theta}$, with a total of 15 components given by [7]:

$$\vec{\theta} = \left(m_1, m_2, \vec{S}_1, \vec{S}_2, \alpha, \delta, \iota, \psi, d_L, t_c, \varphi_c\right), \tag{5.1}$$

where m_i are the masses, $\vec{S}_i$ the spins, α and δ are angles that determine the sky position, ι and ψ are angles that determine the orientation of the orbital plane with respect to the line of sight, d_L is the luminosity distance and t_c and φ_c are respectively the time and phase of coalescence.

Suppose we have some model H, the hypothesis, which is a waveform picked from some family of waveforms $h(\vec{\theta}, t)$, where the family is e.g. the PN approximation for the inspiral. We can then define the likelihood function, $p(d|H, \vec{\theta}, I)$, which is the probability of obtaining the data d, given some hypothesis H, the parameter values $\vec{\theta}$ and whatever background information I we possess. Assuming that the data contains a signal, the so-called signal model $\mathcal{H}_s$, we can split the data up in some noise contribution and some signal contribution which allows us to write it as follows: $d(t) = n(t) + h(\vec{\theta}, t)$. Of course, we can rewrite this to obtain an expression for the noise: $n(t) = d(t) - h(\vec{\theta}, t)$. Furthermore, we assume that the noise is stationary and Gaussian, which allows us to write down the probability distribution for the noise realization [51, 52]:

$$p[n] = \mathcal{N} e^{-\frac{1}{2}(n|n)}, \tag{5.2}$$

where the square brackets denote that $p[n]$ is a functional of n, $\mathcal{N}$ is a normalization factor and the inner product in the exponent is a noise weighted inner product which is defined as follows:

$$(a|b) = 4\mathcal{R}\left[\int_0^\infty df \frac{\tilde{a}^*(f)\,\tilde{b}(f)}{S_n(f)}\right]. \tag{5.3}$$

Here, $\tilde{a}$ and $\tilde{b}$ are the Fourier transformed functions and $\tilde{a}^*$ represents the complex conjugate. $S_n(f)$ is the noise spectral density which assigns the power of the noise as a function of the frequency. The form of $S_n(f)$

depends on the characteristics of the detector. If we now plug into Eq. (5.2) the relation for the noise in terms of the data and the signal, we get an expression for the likelihood:

$$p(d|H,\vec{\theta},I) = \mathcal{N}e^{-\frac{1}{2}(d-h(\vec{\theta})|d-h(\vec{\theta}))}. \tag{5.4}$$

Using this likelihood function, we can compute something called the posterior density distribution (PDF), $p(\vec{\theta}|d,H,I)$, which is the quantity we are interested in. It gives the parameter $\vec{\theta}$ given the data, hypothesis and background information. We can derive it through Bayes' theorem [53]:

$$p(\vec{\theta}|d,H,I) = \frac{p(d|H,\vec{\theta},I)\,p(\vec{\theta}|H,I)}{p(d|H,I)}, \tag{5.5}$$

where $p(\vec{\theta}|H,I)$ is the prior distribution and $p(d|H,I)$ is the evidence. The prior distribution describes knowledge about the parameters $\vec{\theta}$ within a hypothesis H before the data is analyzed. The total prior is an multiplication of the prior for each of the parameters. Most of these are uniform distributions as there is no reason to favour a specific parameter value. Nevertheless, some astrophysically smart choices for the intervals can be made to speed up the calculation. Examples include the component masses, which is constrained to $[1, 100]\ M_\odot$ as GW signals from more massive BHs are outside the range of the detector or the spins, which are naturally limited to $[0, 1]$. The distance is the only non-uniform prior, since it chosen in such a way that the prior is uniform in the volume. The evidence for some hypothesis H is a normalization constant and it does not depend on the parameters $\vec{\theta}$.

In principle, we are now able to calculate the PDF using Eq. (5.5), however, due to the high dimensionality of the parameter space and the rather complicated structure of the likelihood function, this would be a computational nightmare [53]. The next section will explain how we solve this problem.

5.2 Nested Sampling

The nested sampling algorithm is a computational tool designed by Skilling [54] that is used to efficiently calculate the evidence integral over a high-dimensional parameter space. As a by-product of this algorithm, the posterior distribution is computed. Let us begin by defining the evidence integral. Rewriting Bayes' theorem from Eq. (5.5) and integrating over $\vec{\theta}$, which is called marginalizing, yields the following expression:

$$\int d^N\vec{\theta}\, p(\vec{\theta}|d,H,I)p(d|H,I) = \int d^N\vec{\theta}\, p(d|H,\vec{\theta},I)\, p(\vec{\theta}|H,I). \tag{5.6}$$

As the evidence does not depend on $\vec{\theta}$ and the posterior is normalized by definition, we obtain the following expression for the evidence integral:

$$p(d|H,I) = \int d^N\vec{\theta}\, p(d|H,\vec{\theta},I)\, p(\vec{\theta}|H,I) = \int d^N\vec{\theta}\, L(\vec{\theta})\, \pi(\vec{\theta}), \tag{5.7}$$

where we define $L(\vec{\theta})$ as the likelihood function and $\pi(\vec{\theta})$ as the prior distribution. In nested sampling, the evidence integral is computed by rewriting the above integration that depends on the set of N parameters $\vec{\theta}$, in terms of a single scalar called the "prior mass" X. This scalar represents the fraction of the prior volume with a likelihood greater than some value λ. Mathematically, we can write this down as follows:

$$X(\lambda) = \int\int ... \int_{L(\vec{\theta})>\lambda} dX, \tag{5.8}$$

where dX is an element of prior mass:

$$dX = \pi(\theta)d^N\theta. \tag{5.9}$$

So it means that the prior mass is the prior, integrated over a hypervolume in N-dimensional parameter space, which is bounded by a hypersurface of lowest likelihood $L(\vec{\theta}) = \lambda$. Using Eq. (5.8) and Eq. (5.9), we can write the evidence integral from Eq. (5.7) in terms of the prior mass, X:

$$p(d|H,I) = Z = \int\int ... \int d^N\theta L(\vec{\theta})\pi(\theta) = \int \tilde{L}(X)dX, \tag{5.10}$$

where we defined the evidence integral as Z.

The idea behind nested sampling is to construct the function $\tilde{L}(X)$ by progressively finding locations in parameter space with a higher likelihood and thus a smaller prior mass. The evidence, Z, from Eq. (5.10) is approximated by:

$$Z \simeq \sum_{k=1}^{M} L_k \Delta X_k = \sum_{k=1}^{M} L_k (X_{k+1} - X_k). \tag{5.11}$$

From Eq. (5.5), Eq. (5.7) and Eq. (5.11), we can deduce that in terms of the prior mass the PDF is approximated by:

$$p(\vec{\theta}|d, H, I) \simeq \frac{L_k}{Z} \Delta X_k. \tag{5.12}$$

The outline of the algorithm looks as follows:

1. Sample M "live points" $\vec{\theta}_1, \ldots, \vec{\theta}_M$ randomly from the prior $\pi(\vec{\theta})$ and drop them in parameter space. These live points have likelihoods $L(\vec{\theta}_1), \ldots, L(\vec{\theta}_M)$ and are associated with a prior mass.
   We initialise with $Z = 0$, $X_0 = 1$.
2. Record the live point i with lowest likelihood L_i as L_k.
3. Assign a prior mass X_k to the live point i and record it as well.
4. Discard live point i and replace it with a new live point sampled from the prior with a higher likelihood than the lowest remaining one.
5. Execute steps 2 till 4 repeatedly until some termination condition is reached.
6. When the termination condition is reached, calculate the evidence.

There are two issues in the algorithm we have not addressed yet. First of all, how do we assign a prior mass to a live point? Nested sampling does that in a statistical way, namely the prior mass is drawn from some distribution. Say we have just discarded the lowest likelihood point with prior mass X_0 (step 4), we have recorded the new lowest likelihood point (step 2) and we need to assign a prior mass X_1 to that point (step 3). Then the probability that the surface with highest prior mass is at $X = \chi$ is the joint probability that none of the samples have a prior mass $X > \chi$. Since the live points are uniformly sampled from the prior mass and therefore the prior mass is uniform in $[0, 1]$, we can write the probability as [55]:

$$P(X_i < \chi) = \prod_{i=1}^{M} \int_0^{\chi} dX_i = \prod_{i=1}^{M} \chi = \chi^M. \tag{5.13}$$

From this, we can deduce that the probability density that the highest prior mass of M samples has a prior mass of χ is the derivative of the probability from Eq. (5.13), which yields:

$$p(\chi, M) = M\chi^{M-1}. \tag{5.14}$$

In this way, we can assign a prior mass to a live point.

The second issue from the algorithm we have not addressed yet is the termination condition. There is not one single consensus on this subject and we refer to Skilling's paper [54] for a short discussion. In our analysis we have used the termination condition $\Delta Z = 0.1$. ΔZ is an estimate of the evidence still to be accumulated. This quantity is determined by multiplying the highest prior mass of all current live points with the highest likelihood present after every loop in the algorithm. Typical values for the total accumulated evidence from good GW signals are $\log Z \geq 100$, which means our to-be-accumulated evidence of 0.1 is a small fraction of the total. The choice for the specific value 0.1 is arbitrary and the 'best' value is usually found through trial and error.

One may wonder how fast the nested sampling algorithm works, i.e. how fast the area of largest likelihood

is reached. To determine that, it is more convenient to work with the so-called shrinkage ratio, which is the ratio between new and old highest prior mass, i.e. $t = X_k/X_{k-1}$. Making a similar argument as before, the shrinkage ratio can be drawn from a distribution, leaving t with the following probability density distribution:

$$p(t, M) = Mt^{M-1}. \tag{5.15}$$

Working with the shrinkage ratio means that we will assign a new prior mass, by drawing a shrinkage ratio from Eq. (5.15) and multiplying by the old prior mass, i.e. $X_k = t_k X_{k-1}$. Starting off with $X_0 = 1$, the live point with the largest prior mass at the k_{th} iteration is given by:

$$X_k = \prod_{j=1}^{k} t_j. \tag{5.16}$$

The mean and standard deviation of $\log(t)$ then go as [54]:

$$\log(t) = (-1 \pm 1)/M, \tag{5.17}$$

which can be converted to a mean and standard deviation on X_k:

$$\log(X_k) = (-k \pm \sqrt{k})/M. \tag{5.18}$$

We see from Eq. (5.18) that the area in parameter space with highest likelihood is reached exponentially quick and the errors decrease exponentially.

5.3 Resulting bounds on relative charge difference

By adding our constrained parameter $\delta\phi_{-2}$ as an additional 16th component to $\vec{\theta}$, we can use the process of parameter estimation to obtain, with the help of nested sampling, a posterior density distribution for $\delta\phi_{-2}$. We ran the data from the five binary BHs specified earlier and we used the codes from the LIGO Algorithm Library [56]. The waveform model that we used is an Inspiral-Merger-Ringdown waveform model called *IMRPhenomPv2* [57–59], which is an analytical frequency domain model. The inspiral regime of that model is the PN approximation from Section 2.3. Using *LALInference*, the posterior density distribution of each of the parameters is determined. We plotted the probability distributions for $\delta\phi_{-2}$ from the 5 different binary BHs. Moreover, we plotted a Gaussian kernel density estimation over the distribution to create a smooth curve. The plots can be seen in Fig. 4. The red vertical lines show the 90% credible interval from that line to 0. The values corresponding to that credible interval are listed in Table 1, where we also list the 90% upper bounds on $|\xi|$ that are calculated using Eq. (4.40).

	90% credible interval on $\delta\phi_{-2}$	90% upper bound on $\lvert\xi\rvert$
GW150914	$[-0.00980516, 0]$	0.405865
GW151226	$[-0.00263923, 0]$	0.210568
GW170104	$[-0.00700976, 0]$	0.343168
GW170608	$[-0.00616488, 0]$	0.321823
GW170814	$[-0.01229191, 0]$	0.454427

Table 1: 90% credible intervals on $\delta\phi_{-2}$ and 90% upper bounds on $|\xi|$ from 5 different binary BHs. Upper bounds on $|\xi|$ are calculated using Eq. (4.40).

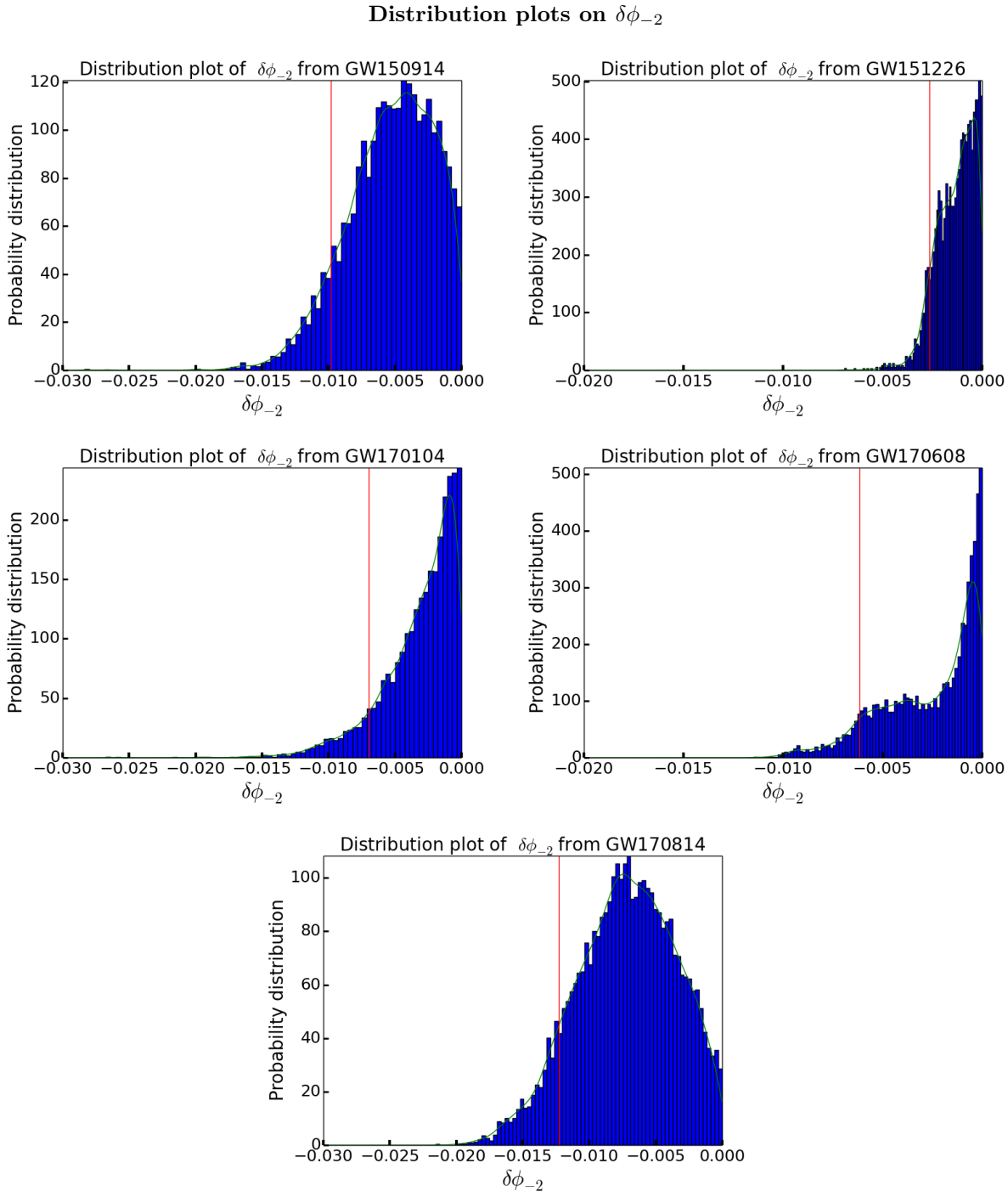

Figure 4: Plots of the constrained $\delta\phi_{-2}$ from the binary BH events considered. The red vertical line indicates the 90% credible bound from that line to 0 and the green line represents the kernel density estimation. Note that the plots from GW151226 and GW170608 already start at -0.020 for visual purposes.

In Fig. 4, we see the probability distribution plots of all five GW events considered and their 90% credible interval. In Bayesian statistics, a 90% credible interval means that there is a 90% probability that the real parameter value lies within that interval, given the observed data [60]. We see that all of the events are consistent with no relative charge difference, i.e. $\delta\phi_{-2} = 0$. While three of the events (GW151226, GW170104, GW170608) have their peak at zero and there seems to be no indication of a relative charge difference, two of the events (GW150914, GW170814) do not peak at zero. At first glance, this may suggest the presence of a relative charge difference. To further investigate this non-zero peak as well as check the robustness of our code, we ran the data from GW150914 again, yet this time without any constraints on $\delta\phi_{-2}$. This plot can be seen on the right of Fig. 5 alongside the distribution plot of the constrained $\delta\phi_{-2}$.

Due to the fact that there are random noise realizations, we expect the peak of the full, unconstrained $\delta\phi_{-2}$ distribution to move back and forth. That means the non-zero peak of the full distribution does not give us much information. If there would be a significant charge difference present in the binary, this should come forward more clearly in the left plot of Fig. 5 as there we constrained $\delta\phi_{-2}$ to test for electric charges. A clearly measurable charge difference would result in a distribution with no support around zero, e.g. a distribution that peaks at -0.025 and goes to 0 at -0.010. This would imply that there is a 0% probability that $\delta\phi_{-2}$ is 0. Comparing the left plot of Fig. 5 to the right plot, we see that the distribution for the constrained $\delta\phi_{-2}$ closely corresponds to the negative regime of the full distribution. We can conclude that there is no indication for any significant relative charge difference. The shifted peak we see in the constrained $\delta\phi_{-2}$ plot is just an artefact of the noise realization that pushes the peak to negative values. The reason the values of the left plot are higher has to do with the normalization of the area under the curve. By comparing the full distribution plot from Fig. 5 to the distribution plot of GW150914 in [50], we can also conclude that our code is correct. Although we did not run the data of the unconstrained $\delta\phi_{-2}$ for GW170814, we can deduce from the plots in [50], that also for this event there is no indication for a significant charge difference.

From the 90% credible intervals, we can set bounds on the relative charge difference. Those are listed in Table 1 and we see all bounds are from the same order of magnitude. We should keep in mind that constraints from individual events are primarily dominated by random noise realizations [50]. In Cardoso et al. [61], they predicted an upper bound of 0.3 on a dimensionless charge-to-mass ratio for GW150914. We see that our upper bound from GW150914 comes close to that value. Furthermore, when we assume that only one component of the binary is charged, we can compare our bounds with the Wald charge from Eq. (3.7) and the extremal charge-to-mass ratio from Eq. (3.3). As the masses of these BH binaries are from the range $10 - 40M_\odot$, we see that even with an extremely strong magnetic field present, the electric charge that can possibly be induced through the Wald mechanism does not come near the bounds found in Table 1. From comparing with the extremal charge-to-mass ratio, we can conclude that we took the upper bound one order of magnitude down.

Distribution plots on constrained and unconstrained $\delta\phi_{-2}$ from GW150914

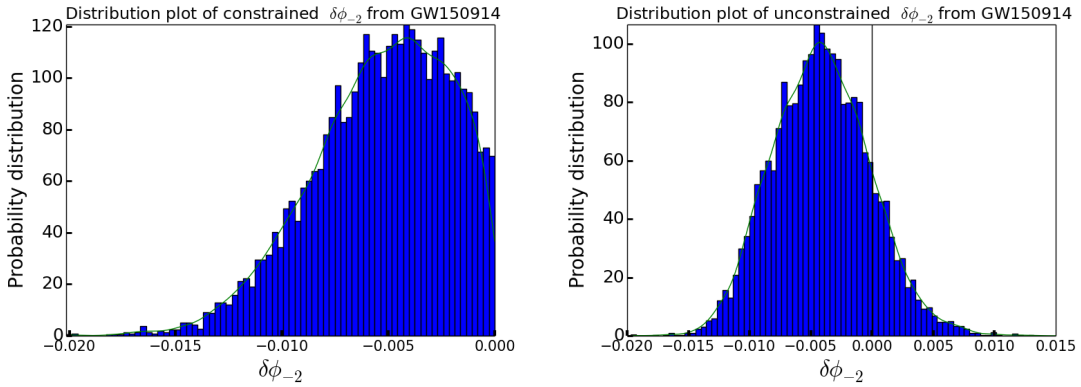

Figure 5: Distribution plots for $\delta\phi_{-2}$ from GW150914. The left plot shows $\delta\phi_{-2}$ constrained to non-positive values only and the right plot shows $\delta\phi_{-2}$ with no constraints.

6 Bounds on charges of a binary pulsar through radio observations

Ever since their first discovery by Hulse and Taylor in 1974 [3], binary pulsars have been a subject of great interest to physicists. They have been used to make excellent cosmic clocks and, more importantly, have been a way to test the strong-field regime of gravitational physics. Pulsars are highly magnetised, rotating neutron stars which emit a beam of electromagnetic radiation along the magnetic dipole axis. As there is generally an inclination angle between the dipole axis and the rotation axis of the pulsar, the pulsar acts as some kind of cosmic light house, emitting pulses once per period that can be detected when the beam is directed towards the earth [62]. A particularly interesting binary pulsar is PSR J0737-3039, discovered in 2004 by Lyne et al. [63]. It is the very first and to this date only double pulsar, which is a binary with two pulsars, that has been discovered. Due to its extremely short orbital period of 2.4 hours, this double pulsar has been a gem for relativistic gravitational physics.

Because of the electromagnetic radiation they emit, binary pulsars can be detected through radio observations. This allows for a detection far earlier in the inspiral than binary BHs, which has consequences for the eccentricity and the bounds as we will see later on. In Section 6.1, we will look at a formalism that can describe the relativistic dynamics of a binary pulsar. Then, in Section 6.2, we will discuss what the effect of electric charges are on the radiated power from a binary pulsar and finally, in Section 6.3, we will discuss the resulting bounds of the double pulsar PSR J0737-3039.

6.1 The post-Keplerian formalism

Periodic variations in the arrival time of a pulse show that some pulsars do not just spin around their own axis, but also orbit some common center of mass [62]. When the orbital velocity is much smaller than the speed of light (non-relativistic system), Newtonian dynamics provide us with the correct motion of the system. We can safely apply Kepler's laws and characterize the orbit by five Keplerian parameters [64]: (1) the orbital period, P_b, (2) the eccentricity, e, (3) the projected semi-major axis, $a_p \sin \iota$, (4) the longitude of periastron, ω and (5) the epoch of passage at periastron, T_0.

Most binary pulsars however, experience relativistic effects due to strong gravitational fields and high orbital velocities. Therefore relativistic corrections for those systems need to be made. These corrections can be modelled in a theory-independent way, adopting the so-called post-Keplerian (PK) parameters. These are purely phenomenological corrections to the non-relativistic orbit, first written down by Damour and Taylor in 1992 [65]. The PK parameters take on the following form in GR (see e.g. [62, 66]), starting off with the relativistic advance of the periastron:

$$\dot{\omega} = 3T_{\odot}^{2/3} \left(\frac{P_b}{2\pi}\right)^{-5/3} \frac{1}{1-e^2}(m_1+m_2)^{2/3}, \tag{6.1}$$

the time dilation and gravitational redshift parameter:

$$\gamma = T_{\odot}^{2/3} e \left(\frac{P_b}{2\pi}\right)^{1/3} \frac{m_1(m_2+2m_1)}{(m_1+m_2)^{4/3}}, \tag{6.2}$$

the rate of orbital decay:

$$\dot{P}_b = -\frac{192\pi}{5} T_{\odot}^{5/3} \left(\frac{P_b}{2\pi}\right)^{-5/3} \frac{\left(1+\frac{73}{24}e^2+\frac{37}{96}e^4\right)}{(1-e^2)^{7/2}} \frac{m_1 m_2}{(m_1+m_2)^{1/3}}, \tag{6.3}$$

the two Shapiro delay parameters:

$$r = T_{\odot} m_2 \tag{6.4}$$

and

$$s = T_{\odot}^{-1/3} \left(\frac{P_b}{2\pi}\right)^{-1/3} x \frac{(m_1+m_2)^{2/3}}{m_2}, \tag{6.5}$$

where in the above expressions m_1 and m_2 are the masses of the two components of the binary (in solar masses), $x = a_p \sin\iota/c$, $s = \sin\iota$ and $T_\odot = GM_\odot/c^3$. The Shapiro delay parameters encompass the effect that in GR, light is not only deflected by gravity, but also slightly delayed when passing through a gravitational field. For a more elaborate explanation on the parameters, we refer to [62]. The beauty of this formalism is that the PK parameters in this form only depend on precisely measurable parameters, the individual masses of the binary and the eccentricity. As the ratio between the masses can be obtained from the Doppler modulation [67], measuring any two PK parameters is sufficient to determine all the parameters on the right hand side of Eqs. (6.1) to (6.5). This means that measuring three or more PK parameters will give us an overdetermined system and the ability to test GR.

6.2 Effect of charge on orbital period

Now that we have an idea on how properties of a binary pulsar are measured, we can study what the effect is when a binary pulsar has some net electric charge accompanied to it. From classical mechanics, we know that there is a relation between the orbital period T and the orbital energy E, which is [15]:

$$T = \text{const.} \times (-E)^{-3/2}. \tag{6.6}$$

In the realm of classical mechanics, there is no time derivative of the orbital period. Taking GWs into account, this is no longer true and we can therefore differentiate Eq. (6.6) with respect to time and divide it by Eq. (6.6) to obtain the following relation:

$$\frac{\dot{T}}{T} = -\frac{3}{2}\frac{\dot{E}}{E}. \tag{6.7}$$

This is the equation that was at the basis for the first indirect evidence for the existence of GWs, as the observations on the orbital period of the Hulse-Taylor binary accurately corresponded to the orbital energy loss, $\dot{E}$, that GWs would cause.

We are going to calculate the orbital energy loss of a binary pulsar as well, however, we are not only going to consider the gravitational radiation, but also the electromagnetic dipole radiation caused by the imposed accelerating electric charges. We are going to neglect the energy loss from the continuous radio pulses as they only extract orbital energy through the slight mass loss they cause (they carry away energy and therefore mass). The situation will be similar to the binary BH system described in Section 2.1, however, we can observe a binary pulsar already in the early stages of inspiral. This means that we have to take the eccentricity of the orbits into account as the binary pulsar will not have had enough time to circularise their orbits. Therefore we do not have a constant radius R as before, but a new equation for the orbit [4] [8]:

$$r^*(\psi) = \frac{a(1-e^2)}{1+e\cos\psi}, \tag{6.8}$$

where a is the semimajor axis, e is the eccentricity and ψ is the true anomaly which denotes the angular position of a body on Keplerian orbit. It is the angle measured counterclockwise from the periapsis to the current position of the orbiting body, as seen from the focus point of the ellipse. For example, $\psi = \pi$ corresponds to the apastron.

Different from the BH binaries, we will only focus on the additional radiated power that is caused by the electric charges. We will see later on that this is sufficient to calculate the bounds. Similar to Section 4.2, we will calculate the electromagnetic radiated power by integrating and averaging over the Poynting vector. In order to obtain the Poynting vector, we first need to derive the electric and magnetic field. The expressions for those are defined as before in Eq. (4.16) and Eq. (4.17), which means we first have to set up the position

[4] The * is added in order to prevent confusion with the r defined before.

vectors for eccentric orbits:

$$\begin{aligned}\vec{x}_1(\psi) &= \frac{\mu}{m_1}\frac{a(1-e^2)}{1+e\cos(\psi)}\begin{pmatrix}\cos\psi\\ \cos\iota\sin\psi\\ 0\end{pmatrix},\\ \vec{x}_2(\psi) &= -\frac{\mu}{m_2}\frac{a(1-e^2)}{1+e\cos\psi}\begin{pmatrix}\cos\psi\\ \cos\iota\sin\psi\\ 0\end{pmatrix}.\end{aligned} \tag{6.9}$$

To derive the electric and magnetic field, we need the second time derivative of those, which are given by:

$$\begin{aligned}\ddot{\vec{x}}_1 &= -\frac{\mu}{m_1}\frac{GM}{a^2}\frac{(1+e\cos\psi)^2}{(1-e^2)^2}\begin{pmatrix}\cos\psi\\ \cos\iota\sin\psi\\ 0\end{pmatrix},\\ \ddot{\vec{x}}_2 &= \frac{\mu}{m_2}\frac{GM}{a^2}\frac{(1+e\cos\psi)^2}{(1-e^2)^2}\begin{pmatrix}\cos\psi\\ \cos\iota\sin\psi\\ 0\end{pmatrix},\end{aligned} \tag{6.10}$$

where we used [8]:

$$\dot{\psi} = \left(\frac{GM}{a^3}\right)^{1/2}(1-e^2)^{-3/2}(1+e\cos\psi)^2. \tag{6.11}$$

Analogous to Section 4.2, we can now compute the fields:

$$\vec{E} \simeq \frac{1}{4\pi\epsilon_0}\frac{1}{c^2 r}\frac{GM\mu}{a^2}\left(\frac{q_1}{m_1}-\frac{q_2}{m_2}\right)\frac{(1+e\cos\psi)^2}{(1-e^2)^2}\begin{pmatrix}\cos\psi\\ \cos\iota\sin\psi\\ 0\end{pmatrix}, \tag{6.12}$$

$$\vec{B} \simeq -\frac{1}{4\pi\epsilon_0}\frac{1}{c^3 r}\frac{GM\mu}{a^2}\left(\frac{q_1}{m_1}-\frac{q_2}{m_2}\right)\frac{(1+e\cos\psi)^2}{(1-e^2)^2}\begin{pmatrix}\cos\iota\sin\psi\\ -\cos\psi\\ 0\end{pmatrix}. \tag{6.13}$$

Subsequently, the Poynting vector will be calculated according to Eq. (4.21), where we see that the dimensionless variable ξ^2 from Eq. (4.23) will arise again:

$$\vec{S} = \frac{1}{\mu_0}\frac{1}{4\pi\epsilon_0}\frac{1}{c^5 r^2}\frac{G^3M^2\mu^2}{a^4}\xi^2\frac{(1+e\cos\psi)^4}{(1-e^2)^4}\begin{pmatrix}0\\ 0\\ \cos^2\psi+\cos^2\iota\sin^2\psi\end{pmatrix}. \tag{6.14}$$

We now integrate the absolute value of the Poynting vector over any surface surrounding the dipole (see Eq. (4.25)), which yields:

$$P_{dip}(\psi) = \frac{1}{2}\frac{G^3\mu^2M^2(1+e\cos\psi)^4}{c^3a^4(1-e^2)^4}\xi^2(2\cos^2\psi+\frac{2}{3}\sin^2\psi). \tag{6.15}$$

Again, we compute the average to obtain the actual radiated power:

$$P_{dip} \equiv \frac{1}{T}\int_0^T dtP(\psi) = \frac{\omega_0}{2\pi}\int_0^{2\pi}\frac{d\psi}{\dot{\psi}}P(\psi) = (1-e^2)^{3/2}\int_0^{2\pi}\frac{d\psi}{2\pi}(1+e\cos\psi)^{-2}P(\psi), \tag{6.16}$$

where we used the expression for $\dot{\psi}$ from Eq. (6.11) and we used Kepler's third law, but now for eccentric orbits:

$$\omega_0^2 = \frac{GM}{a^3}. \tag{6.17}$$

By substituting Eq. (6.15) into Eq. (6.16) and solving the integral, we obtain the following result for the radiated power:

$$\begin{aligned} P_{dip} &= \frac{1}{2}\frac{G^3\mu^2M^2}{c^3a^4(1-e^2)^{5/2}}\xi^2\int_0^{2\pi}\frac{d\psi}{2\pi}(1+e\cos\psi)^2(2\cos^2\psi+\frac{2}{3}\sin^2\psi) \\ &= \frac{1}{2}\frac{G^3\mu^2M^2}{c^3a^4(1-e^2)^{5/2}}\xi^2\left[\frac{1}{2\pi}\frac{\pi}{3}(8+5e^2)\right] \\ &= \frac{2}{3}\frac{G^3\mu^2M^2}{c^3a^4}\xi^2 g(e), \end{aligned} \tag{6.18}$$

with $g(e)$ defined as follows:

$$g(e) = \frac{1}{(1-e^2)^{5/2}}\left(1+\frac{5}{8}e^2\right). \tag{6.19}$$

Using relation Eq. (6.17) to rewrite Eq. (6.18) yields:

$$P_{dip} = \frac{2}{3}\frac{G\mu^2a^2\omega_0^4}{c^3}\xi^2 g(e). \tag{6.20}$$

From this expression, we can observe that for $e = 0$, $g(e)$ becomes 1, while a turns into the radius of a circular orbit and we get back exactly our result for the BH binary from Eq. (4.26).

To calculate to total power, we need the gravitational radiated power in the case of eccentric orbits, which is given by (this was first derived by Peters and Mathews [13]):

$$P_{GW} = \frac{32G^4\mu^2M^3}{5c^5a^5}f(e), \tag{6.21}$$

where $f(e)$ is defined as follows:

$$f(e) = \frac{1}{(1-e^2)^{7/2}}\left(1+\frac{73}{24}e^2+\frac{37}{96}e^4\right). \tag{6.22}$$

As we assume that that the radiation due to electric charges is small compared to the GW radiation, we write it as a small correction to the GW radiation:

$$\begin{aligned} \dot{E} = P_{GW} + P_{dip} &= \frac{32G^4\mu^2M^3}{5c^5a^5}f(e) + \frac{2}{3}\frac{G^3\mu^2M^2}{c^3a^4}\xi^2 g(e) \\ &= P_{GW}\left(1+\frac{10}{96}\frac{\xi^2}{(\frac{GM}{c^2a})}\frac{g(e)}{f(e)}\right) \\ &= P_{GW}\left(1+\frac{10}{96}\xi^2\frac{c^2}{v^2}\frac{g(e)}{f(e)}\right), \end{aligned} \tag{6.23}$$

where in the last step v is the characteristic orbital velocity, which is calculated using Kepler's law in the form of Eq. (2.27) and Eq. (6.17):

$$v = \sqrt{\frac{GM}{a}}. \tag{6.24}$$

6.3 Resulting bound of the double pulsar PSR J0737-3039

The additional term in the total radiated power from Eq. (6.23) can be used to constrain the relative charge difference ξ of the particular double pulsar PSR J0737-3039. To derive this bound, we parametrise the power as in Barausse et al. [68] in their pursuit to constrain dipolar emission for alternative theories of gravity:

$$\dot{E}_{GW} = \dot{E}_{GR}\left[1 + B\left(\frac{GM}{r_{12}c^2}\right)^{-1}\right], \tag{6.25}$$

where $\dot{E}_{GR}$ is the GW power according to GR, M is the total mass of the binary, r_{12} is the orbital separation and B is a theory-dependent parameter governing the strength of some dipole term. As the orbital separation is twice the semimajor axis a, we can use Eq. (6.24) to rewrite the parameterisation as:

$$\dot{E}_{GW} = \dot{E}_{GR}\left[1 + 2B\frac{c^2}{v^2}\right]. \tag{6.26}$$

Comparing with Eq. (6.23) allows us to extract the component B in the case of electromagnetic dipole radiation, as $P_{GW} = \dot{E}_{GR}$. We obtain:

$$B = \frac{5}{96}\frac{g(e)}{f(e)}\xi^2. \tag{6.27}$$

In order to pick up deviations from GR in GW data or abnormalities in general, Yunes and Pretorius have developed the so-called Parameterized post-Einsteinian Framework [69]. This framework also allows for measurements on how precise a GW event is purely described by GR. In further work, Yunes and Hughes [70] have set binary pulsar constraints on the Parameterized post-Einsteinian Framework using the accurate measurements on the PK parameters from e.g. the double pulsar [63, 64, 71]. These binary pulsar constraints have been transformed to an upper bound on B by Barausse et al. [68]. For the double pulsar PSR J0737-3039, this leads to an upper bound of $|B| \lesssim 6 \times 10^{-8}$. Using Eq. (6.27), we apply this constraint to set a bound on the relative charge difference ξ:

$$|\xi| = \frac{1}{\sqrt{4\pi\epsilon_0 G}}\left|\left(\frac{q_1}{m_1} - \frac{q_2}{m_2}\right)\right| \lesssim 0.00108742, \tag{6.28}$$

where we used the eccentricity $e = 0.0877775(9)$ as given in Kramer et al. [64].

We see that this bound is much more stringent than the bounds we found for the BH binaries in Section 5.3. This has to do with the detection early in the inspiral we mentioned earlier. Once detected, the binary pulsar can be tracked over many years, which leads to very precise observations and therefore a tighter bound. To give an idea on the scale of such a charge-to-mass ratio, we assume for simplicity that only the heaviest pulsar of the two ($m_1 = 1.3381 M_\odot$ [64]) is charged. Rewriting Eq. (6.28) and filling in m_1, ϵ_0, G, leads to $q_1 = 2.49398 \times 10^{17} C$. As such large values of charge may still not be very imaginable, we ask the reader to visualise the following situation. Suppose every human on this planet got their hands on the new Tesla model S electric car. One day, everyone is going to drive that car from fully charged until fully discharged. Besides the hazard of children behind the wheel and enormous traffic jams, the amount of charge that we constrained on the double pulsar is comparable to the amount of charge that would run through all those car batteries. 41 times.

7 Projected bounds for the future Einstein Telescope

In anticipation of a completely operational Einstein telescope [72], we are going to estimate projected bounds on the relative electric charge difference of BH binaries. In order to achieve those bounds, we adopt the Fisher matrix formalism which allows for a quick estimation on the measurement uncertainty of a given parameter. This formalism is frequently used in the field of GW analysis as a first approximation tool to test the accuracy of parameter estimation [73].

It should be pointed out straight away that the Fisher matrix formalism has its limitations [74]. On top of that, we will not even use it in its full potential, e.g. we will only include the inspiral waveform model (PN approximation) instead of inspiral-merger-ringdown waveform models and we will not account for multiple detectors with different orientations. All these shortcomings are the reason why we will only use the Fisher matrix formalism as a rough estimate. One notorious weakness of the Fisher matrix formalism we will point out here, is bad estimates at a low signal-to-noise ratio (SNR). This can, for example, be seen in Fig. 2 of [74] where Vallisneri plots a so-called mismatch ratio, which is the ratio between the linearised approximation of the Fisher matrix formalism and the real waveform model. Although we can not directly compare our case to the plot from Vallisneri due to different masses and parameters, we can clearly see that a higher SNR results in higher accuracy. The Einstein telescope, which classifies as a so-called third generation detector, is expected to have a 10 times greater SNR than Advanced LIGO for the same events [75]. This gives us some faith that the Fisher matrix formalism provides reasonably good estimates for the Einstein Telescope. We will be testing 5 parameters, $(t_c, \phi_c, \mathcal{M}_c, \eta, \xi)$, where our parameter of interest is ξ. In Section 7.1, we will derive the Fisher Information Matrix and afterwards, in Section 7.2, we will estimate the projected bounds on our dimensionless charge difference parameter.

7.1 Derivation Fisher Information Matrix

The starting point of the derivation lies at the expression for the Gaussian likelihood function we derived earlier in Eq. (5.4). When we assume an uniform prior distribution, otherwise called a 'flat prior', i.e. $p(\vec{\theta}|H, I)$ is constant, we can use Bayes' theorem from Eq. (5.5) to write the following [5]:

$$p(\vec{\theta}|d, H, I) \propto p(d|\vec{\theta}, H, I) = \mathcal{N} e^{-\frac{1}{2}(d-h(\vec{\theta})|d-h(\vec{\theta}))}. \tag{7.1}$$

In general, $\vec{\theta}$ gives us a probability distribution for each parameter that peaks at some point. We define this point as the point of maximum likelihood and it is associated with a value θ_{ML}. In the Fisher matrix formalism, the assumption is made that this value is equal to real value of the parameter. Usually, this is not true due to noise realizations that cause an offset. Nevertheless, we use this assumption and write $\vec{\theta}$ as follows:

$$\vec{\theta} = \vec{\theta}_{ML} + \delta\vec{\theta}, \tag{7.2}$$

where $\delta\vec{\theta}$ is some deviation from the maximum likelihood. Next, we are going to use this relation and substitute it into Eq. (7.1). As there does not exist such a thing as a probability distribution for a single point, the probability distribution will just be for $\delta\vec{\theta}$ and given by (we will drop the factors behind the vertical bar; these will be implied from now on):

$$p(\delta\vec{\theta}) = \mathcal{N}' e^{-\frac{1}{2}(d-h(\vec{\theta}) \mid d-h(\vec{\theta}))} = e^{-\frac{1}{2}(d \mid d)+(d \mid h(\vec{\theta}))-\frac{1}{2}(h(\vec{\theta} \mid h(\vec{\theta}))}, \tag{7.3}$$

where $\mathcal{N}'$ is a normalization factor. Taking the logarithm on both sides yields:

$$\log p(\delta\vec{\theta}) = (d \mid h(\vec{\theta})) - \frac{1}{2}(h(\vec{\theta}) \mid h(\vec{\theta})) + \text{const.}\,, \tag{7.4}$$

where we added $(d|d)$ to the constant term as it is not dependent on $\delta\vec{\theta}$. To obtain a workable expression for $p(\delta\vec{\theta})$, we need to expand the signal, $h(\vec{\theta})$, up to second order around the maximum likelihood values:

$$h(\vec{\theta}) = h(\vec{\theta}_{ML}) + \left.\frac{\partial h}{\partial \theta^i}\right|_{ML} \delta\theta^i + \frac{1}{2}\left.\frac{\partial^2 h}{\partial\theta^i \partial\theta^j}\right|_{ML} \delta\theta^i\delta\theta^j, \tag{7.5}$$

[5] Remember that the inner product in the exponent is actually the noise weighted inner product defined in Eq. (5.3).

where we use the Einstein summation convention. When we substitute the expansion from Eq. (7.5) into Eq. (7.4), we obtain (the dependency of h on $\vec{\theta}$ is implied):

$$\begin{aligned}\log p(\delta\vec{\theta}) &= (d \mid h) - \frac{1}{2}(h \mid h) + \text{const.} \\ &= (d \mid h)|_{ML} + \left(d \mid \frac{\partial h}{\partial \theta^i}\right)\Bigg|_{ML} \delta\theta^i + \frac{1}{2}\left(d \mid \frac{\partial^2 h}{\partial\theta^i \partial\theta^j}\right)\Bigg|_{ML} \delta\theta^i\delta\theta^j - \frac{1}{2}(h \mid h)|_{ML} \\ &- \left(h \mid \frac{\partial h}{\partial \theta^i}\right)\Bigg|_{ML} \delta\theta^i - \frac{1}{2}\left(h \mid \frac{\partial^2 h}{\partial\theta^i \partial\theta^j}\right)\Bigg|_{ML} \delta\theta^i\delta\theta^j - \frac{1}{2}\left(\frac{\partial h}{\partial\theta^i} \mid \frac{\partial h}{\partial\theta^j}\right)\Bigg|_{ML} \delta\theta^i\delta\theta^j + \text{const.} \end{aligned} \tag{7.6}$$

To simplify this term, we add all terms independent of $\delta\vec{\theta}$ to the constant term. Moreover, taking the derivative of Eq. (7.4) with respect to θ_i at the point of maximum likelihood, yields the following condition:

$$\frac{\partial}{\partial\theta^i}\left(\log p(\delta\vec{\theta})\right)\Big|_{ML} = 0 = \left(d \mid \frac{\partial h}{\partial\theta^i}\right)\Bigg|_{ML} - \left(h \mid \frac{\partial h}{\partial\theta^i}\right)\Bigg|_{ML}. \tag{7.7}$$

This condition helps us to simplify Eq. (7.6) further:

$$\begin{aligned}\log p(\delta\vec{\theta}) &= (d \mid h) - \frac{1}{2}(h \mid h) + \text{const.} \\ &= \frac{1}{2}\left(d \mid \frac{\partial^2 h}{\partial\theta^i \partial\theta^j}\right)\Bigg|_{ML} \delta\theta^i\delta\theta^j - \frac{1}{2}\left(h \mid \frac{\partial^2 h}{\partial\theta^i \partial\theta^j}\right)\Bigg|_{ML} \delta\theta^i\delta\theta^j - \frac{1}{2}\left(\frac{\partial h}{\partial\theta^i} \mid \frac{\partial h}{\partial\theta^j}\right)\Bigg|_{ML} \delta\theta^i\delta\theta^j + \text{const.} \\ &= \frac{1}{2}\left(n \mid \frac{\partial^2 h}{\partial\theta^i \partial\theta^j}\right)\Bigg|_{ML} \delta\theta^i\delta\theta^j - \frac{1}{2}\left(\frac{\partial h}{\partial\theta^i} \mid \frac{\partial h}{\partial\theta^j}\right)\Bigg|_{ML} \delta\theta^i\delta\theta^j + \text{const.}, \end{aligned} \tag{7.8}$$

where we used the relation $d = n + h(\vec{\theta})$.

The two terms from Eq. (7.8) that we are now left with, do not have a similar contribution to the probability distribution. In order to prove that, we should take a look at how these two noise-weighted inner products from Eq. (7.8) compare to the SNR. The SNR is defined as follows [22]:

$$\text{SNR}^2 = 4\int_0^\infty df \frac{|\tilde{h}(f)|^2}{S_h(f)}. \tag{7.9}$$

Filling the term for $\tilde{h}(f)$ from Eq. (2.28) into Eq. (7.9), we see that $e^{i\Psi}$ falls out due to the absolute square. Furthermore, the squared amplitude $\mathcal{A}^2$ can be taken outside of the integral as it is independent of f [6]. The definite integral that remains, will just produce a value which means the SNR is proportional to $\mathcal{A}$, i.e. $\text{SNR} \propto \mathcal{A}$. We can use this proportionality, to link both terms from Eq. (7.8) to the SNR. Writing out the noise-weighted inner product for the first term, we see that, following the same argument as before, the first term is proportional to $\mathcal{A}$ and thus proportional to the SNR. The second term however, is proportional to $\mathcal{A}^2$ and thus to SNR^2. To detect a GW, a SNR of at least 8 is required, but higher SNR are preferable. Therefore the second term in Eq. (7.8) is dominant (especially at high SNR) and we will allow ourselves to neglect the first term. As a result of that, we can write the probability distribution from Eq. (7.3) in the following way:

$$p(\delta\vec{\theta}) = \mathcal{N}'' e^{-\frac{1}{2}\Gamma^{ij}\delta\theta^i\delta\theta^j}, \tag{7.10}$$

where $\mathcal{N}''$ is the appropriate normalization constant and we define the Fisher Information Matrix as:

$$\Gamma^{ij} = \left(\frac{\partial h}{\partial\theta^i} \mid \frac{\partial h}{\partial\theta^j}\right)\Big|_{ML}. \tag{7.11}$$

[6] Recall from Sec. 2.3 that $\mathcal{A} \propto \mathcal{M}_c^{5/6} Q(\text{angles})/r$.

From Eq. (7.10), we see that the deviations from maximum likelihood follow a Gaussian distribution and we can look for the 1-sigma spread of $\delta\vec{\theta}$. When we set $i = j$ and compare Eq. (7.10) to a normal Gaussian distribution, it is evident that the variance is equal to the diagonal of the inverse Fisher Information Matrix, i.e. $(\sigma^i)^2 = (\Gamma^{ii})^{-1}$. In general, the inverse of the Fisher Information Matrix is equal to the variance-covariance matrix, i.e. $\Sigma^{ij} = (\Gamma^{ij})^{-1}$ [73]. As we are not interested in the covariance between parameters, we only have to focus on the diagonal of the variance-covariance matrix. The 1-sigma error is then given by:

$$\sigma^i = \sqrt{\Sigma^{ii}}. \tag{7.12}$$

7.2 Projected bounds

Using the Fisher matrix formalism, we can calculate the 1-sigma error for any given parameter. We assume that there is no relative charge difference, i.e. our variable $\xi = 0$, and compute the Fisher Information Matrix using *Mathematica*. We do this for both Advanced LIGO and Einstein Telescope[7] for comparison reasons. The results are shown in Table 2. We rescaled the 1-sigma error (68%) to a 90% bound, so we can compare our results with the bounds found in Section 5.3. Moreover, for the Advanced LIGO case, we corrected for the actual SNR that was found by the Advanced LIGO detectors [11].

	68% $\|\xi\|$ AL	90% $\|\xi\|$ AL	68% $\|\xi\|$ ET	90% $\|\xi\|$ ET
GW150914	0.154412	0.204368	0.00535768	0.00709105
GW151226	0.0446890	0.0591473	0.00189595	0.00250936
GW170104	0.229230	0.303392	0.0106596	0.0141083
GW170608	0.0290295	0.0384213	0.00272670	0.00360887
GW170814	0.148469	0.196503	0.00529081	0.00700254

Table 2: Table of the values found for the 1-sigma and 90% bounds for Advanced LIGO and Einstein Telescope using the Fisher matrix formalism. The events used are the same as Section 5.3. AL = Advanced LIGO, ET = Einstein Telescope.

Comparing the results for the 90% bound of Advanced LIGO from Table 2 with the results found in Section 5.3, we see that the Fisher formalism produces reasonably good results. For three out of five events, we achieve the right order of magnitude and for the other two we are one order of magnitude off. However, as argued, we cannot attach too much weight to these results. The results for Einstein Telescope are more trustworthy due to the expected high SNR and we see that bounds are expected to drop one or two orders of magnitude compared to Table 1. Furthermore, the bounds reach the same order of magnitude as the bound on the double pulsar from Eq. (6.28), which is remarkable since the double pulsar has been tracked for over a decade.

The projected Einstein Telescope bounds have reached such a low value that we can compare the projected bounds to the Wald charge from Section 3.2. When we assume for simplicity only one of the two components of a binary accumulates charges, the charge-to-mass ratio due to Wald charge from e.g. GW150914 can be calculated using Eq. (3.7). Taking into account the $1/\sqrt{4\pi}$, assuming a magnetic field of $10^{15}G$ and using the mass of the heaviest BH of GW150914 ($35.6M_\odot$), we obtain a value of $(1/\sqrt{4\pi\epsilon_0 G})Q/M \approx 0.0000687139$. Although this is still two orders of magnitude below the projected bound for Einstein telescope, further improvements on the telescope or more extreme cosmic events may enable us to observe Wald charge through GW observations.

[7] Many thanks to Quint Lafleur and Gideon Koekoek for providing me with the sensitivity curve for respectively Advanced LIGO and Einstein Telescope.

8 Conclusions

In this thesis, we have presented a way to constrain the relative electric charge difference of binary BHs and binary neutron stars through GW observations. Both BHs and neutron stars are expected to be electrically neutral to good approximation, however, we have seen that this does not a priori has to be true for all binaries.

We studied the dominant effect of electric charges on the gravitational waveform by deriving what the additional energy and radiated power terms are up to leading order in small quantities. We showed that there arises an extra term in the phase, which compared to the PN approximation, is a -1PN term. This term includes a relative electric charge difference between the two components of the binary and can only take on non-positive values.

Exploiting this new feature of the -1PN term, we used data from five different binary BH GW events to set upper bounds on the relative charge difference. We added the constrained coefficient of the -1PN term to the parameter space and used the process of parameter estimation to obtain probability distributions on $\delta\phi_{-2}$ for the five events considered. From these distributions, we concluded that for all of the events there is no indication for a significant relative charge difference. We placed 90% credible intervals on the probability distributions and derived 90% upper bounds on the dimensionless relative charge difference. All of these bounds are in the order of 10^{-1}, which means we took the bounds one order of magnitude down from the theoretical limit.

We proceeded by deriving once again what the influence of electric charges on the orbital motion is, but now in the case of a binary pulsar. We calculated the additional radiated power and we saw that the same dimensionless relative charge difference arises. Through radio observations on the double pulsar PSR J0737-3039, we derived an upper bound on this parameter, which is in the order of 10^{-3}. We concluded that this bound is more stringent than the bounds on the binary BHs because the double pulsar has been tracked and measured for over a decade.

Finally, we employed the Fisher matrix formalism to estimate projected bounds that can be obtained once the Einstein Telescope becomes active. We saw that bounds are expected to drop one or two orders of magnitude, which is still two orders of magnitude below realistic values of Wald charge the considered binary BHs would induce.

Coming back to our research question, we see that it is possible to obtain an upper bound on a quantity that describes the electric charge difference of a binary through GW observations. The relative charge difference provides us with information on the properties of a binary. It can be used to study differences between the two components of the binary, e.g. differences in magnetic field. However, information from a relative charge difference is limited to the binary as a whole and we have used the assumption that only one of the components in the binary is charged multiple times in this work. More information could be obtained by constraining the electric charge of the individual components of the binary. We did not manage to obtain such bounds but this may be interesting for future work. We expect that this can be realised by including the merger and ringdown in the calculations. The ringdown GWs should contain information about the newly formed single BH (or neutron star), which would possibly lead to an upper bound on the total charge-to-total mass ratio. This ratio can be used in combination with the relative charge difference found in this work to obtain an upper bound on the electric charges of the individual components of a binary.

We are only at the start of an exciting era for gravitational wave physics. Many years of theoretical research and improvements on detectors have led us to the point that we are now able to detect these waves and extract physics from them. Continuing this effort will allow physicists to discover many more events and we hope that, among other things, more stringent bounds can be placed on the electric charges of binary systems.

I bet the square inside Edwin A. Abbott's head would never have thought how much there is lurking inside a new dimension.

Acknowledgments

First of all I would like to express my sincere gratitude and great appreciation to my supervisor prof. dr. Chris van den Broeck for his guidance, advise and valuable insights. I truly enjoyed our weekly meetings. Furthermore, this research has made use of data, software and/or web tools obtained from the Gravitational Wave Open Science Center (https://www.gw-openscience.org), a service of LIGO Laboratory, the LIGO Scientific Collaboration and the Virgo Collaboration. LIGO is funded by the U.S. National Science Foundation. Virgo is funded by the French Centre National de Recherche Scientifique (CNRS), the Italian Istituto Nazionale della Fisica Nucleare (INFN) and the Dutch Nikhef, with contributions by Polish and Hungarian institutes.

References

[1] International Centre for Theoretical Physics, https://www.icts.res.in/program/gws2020, **2020**.

[2] B. P. Abbott et al., "Observation of Gravitational Waves from a Binary Black Hole Merger", *Phys. Rev. Lett.* **2016**, *116 no. 6*, 061102.

[3] R. A. Hulse, J. H. Taylor, "Discovery of a pulsar in a binary system.", *The Astrophysical Journal* **1975**, *195*, L51–L53.

[4] A. Einstein, "On the General Theory of Relativity", *Sitzungsber. Preuss. Akad. Wiss. Berlin (Math. Phys.)* **1915**, 778–786.

[5] E. E. Flanagan, S. A. Hughes, "The Basics of gravitational wave theory", *New J. Phys.* **2005**, *7*, 204.

[6] K. D. Kokkotas, "Gravitational waves Physics", *Acta Phys. Polon. B* **2007**, *38*, 3891–3923.

[7] C. van den Broeck, Lecture slides on gravitational waves, University of Groningen, **2019**.

[8] M. Maggiore, *Gravitational Waves. Vol. 1: Theory and Experiments*, Oxford University Press, **2007**.

[9] M. Pitkin, S. Reid, S. Rowan, J. Hough, "Gravitational Wave Detection by Interferometry (Ground and Space)", *Living Rev. Rel.* **2011**, *14*, 5.

[10] LIGO Timeline, https://www.ligo.caltech.edu/page/timeline, **2020**.

[11] B. Abbott et al., "GWTC-1: A Gravitational-Wave Transient Catalog of Compact Binary Mergers Observed by LIGO and Virgo during the First and Second Observing Runs", *Phys. Rev. X* **2019**, *9*, 031040.

[12] A. Buonanno, "Gravitational waves from inspiraling binary black holes", *Class. Quant. Grav.* **2002**, *19*, 1267–1278.

[13] P. C. Peters, J. Mathews, "Gravitational Radiation from Point Masses in a Keplerian Orbit", *Phys. Rev.* **1963**, *131*, 435–440.

[14] T. G. F. Li, *Extracting Physics from Gravitational Waves: Testing the Strong-field Dynamics of General Relativity and Inferring the Large-scale Structure of the Universe*, Springer International Publishing Ag, **2016**.

[15] D. Morin, *Introduction to Classical Mechanics: With Problems and Solutions*, Cambridge University Press, **2008**.

[16] W. Becker, *Neutron Stars and Pulsars*, *Vol. 357*, **2009**, p. 652.

[17] R. Essick, S. Vitale, M. Evans, "Frequency-dependent responses in third generation gravitational-wave detectors", *Phys. Rev. D* **2017**, *96*, 084004.

[18] M. Rakhmanov, J. D. Romano, J. T. Whelan, "High-frequency corrections to the detector response and their effect on searches for gravitational waves", *Classical and Quantum Gravity* **2008**, *25*, 184017.

[19] S. Droz, D. J. Knapp, E. Poisson, B. J. Owen, "Gravitational waves from inspiraling compact binaries: Validity of the stationary phase approximation to the Fourier transform", *Phys. Rev. D* **1999**, *59*, 124016.

[20] A. Buonanno, B. Iyer, E. Ochsner, Y. Pan, B. Sathyaprakash, "Comparison of post-Newtonian templates for compact binary inspiral signals in gravitational-wave detectors", *Phys. Rev. D* **2009**, *80*, 084043.

[21] H. Asada, T. Futamase, "PostNewtonian approximation: Its Foundation and applications", *Prog. Theor. Phys. Suppl.* **1997**, *128*, 123–181.

[22] K. Arun, B. R. Iyer, B. Sathyaprakash, P. A. Sundararajan, "Parameter estimation of inspiralling compact binaries using 3.5 post-Newtonian gravitational wave phasing: The Non-spinning case", *Phys. Rev. D* **2005**, *71*, 084008.

[23] L. Blanchet, G. Faye, B. R. Iyer, B. Joguet, "Gravitational-wave inspiral of compact binary systems to 7/2 post-Newtonian order", *Phys. Rev. D* **2002**, *65*, 061501.

[24] T. Damour, B. R. Iyer, B. S. Sathyaprakash, "Comparison of search templates for gravitational waves from binary inspiral", *Phys. Rev. D* **2001**, *63*, 044023.

[25] T. Damour, B. R. Iyer, B. S. Sathyaprakash, "Comparison of search templates for gravitational waves from binary inspiral: 3.5PN update", *Phys. Rev. D* **2005**, *72*, 029901.

[26] C. W. Misner, K. Thorne, J. Wheeler, *Gravitation*, W. H. Freeman, San Francisco, **1973**.

[27] M. Zajaček, A. Tursunov, A. Eckart, S. Britzen, E. Hackmann, V. Karas, Z. Stuchlík, B. Czerny, J. A. Zensus, "Constraining the charge of the Galactic centre black hole", *J. Phys. Conf. Ser.* **2019**, *1258*, 012031.

[28] T. Adamo, E. Newman, "The Kerr-Newman metric: A Review", *Scholarpedia* **2014**, *9*, 31791.

[29] S. B. Giddings, A. Strominger, "Dynamics of extremal black holes", *Phys. Rev. D* **1992**, *46*, 627–637.

[30] J. Levin, D. J. D'Orazio, S. Garcia-Saenz, "Black Hole Pulsar", *Phys. Rev. D* **2018**, *98*, 123002.

[31] B. Zhang, "Charged Compact Binary Coalescence Signal and Electromagnetic Counterpart of Plunging Black Hole–Neutron Star Mergers", *Astrophys. J. Lett.* **2019**, *873*, L9.

[32] Z. Dai, "Inspiral of a Spinning Black Hole–Magnetized Neutron Star Binary: Increasing Charge and Electromagnetic Emission", *Astrophys. J. Lett.* **2019**, *873*, L13.

[33] J. Bally, E. R. Harrison, "The electrically polarized universe", *Astrophys. J.* **1978**, *220*, 743.

[34] A. S. Eddington, *The Internal Constitution of the Stars*, **1926**.

[35] A. Eckart et al., "Flare emission from Sagittarius A*", *J. Phys. Conf. Ser.* **2012**, *372*, 012022.

[36] M. Zajaček, A. Tursunov, "Electric charge of black holes: Is it really always negligible?", **2019**.

[37] R. M. Wald, "Black hole in a uniform magnetic field", *Phys. Rev. D* **1974**, *10*, 1680–1685.

[38] H. Kim, C. H. Lee, H. K. Lee, "Nonvanishing magnetic flux through the slightly charged Kerr black hole", *Phys. Rev. D* **2001**, *63*, 064037.

[39] H. K. Lee, C. H. Lee, M. H. van Putten, "Electric charge and magnetic flux on rotating black holes in a force-free magnetosphere", *Mon. Not. Roy. Astron. Soc.* **2001**, *324*, 781.

[40] G. Salvesen, P. J. Armitage, J. B. Simon, M. C. Begelman, "Strongly Magnetized Accretion Disks Around Black Holes", American Astronomical Society Meeting Abstracts **2017**, *229*.

[41] M. de Kool, G. V. Bicknell, Z. Kuncic, "Magnetic Fields in Accretion Disks*", **1999**, *16*, 225–233.

[42] H. K. Lee, R. Wijers, G. Brown, "Blandford-znajek process as a gamma-ray burst central engine", *ASP Conf. Ser.* **1999**, *190*, 173.

[43] R. D. Blandford, R. L. Znajek, "Electromagnetic extraction of energy from Kerr black holes", *Monthly Notices of the Royal Astronomical Society* **1977**, *179*, 433–456.

[44] B. S. Ryden, B. M. Peterson, *Foundations of astrophysics*, Pearson Addison-Wesley, **2010**.

[45] M. Y. Piotrovich, Y. N. Gnedin, N. A. Silant'ev, T. M. Natsvlishvili, S. D. Buliga, "Magnetic field and radius of the innermost stable circular orbit near super-massive black holes in active galactic nuclei", *Astronomische Nachrichten* **2015**, *336*, 1013–1016.

[46] A. Tursunov, Z. Stuchlík, M. Kološ, N. Dadhich, B. Ahmedov, "Supermassive black holes as possible sources of ultra high energy cosmic rays", *Astrophys. J.* **2020**, *895*, 14.

[47] B. R. Iyer, C. M. Will, "Post-Newtonian gravitational radiation reaction for two-body systems: Non-spinning bodies", *Phys. Rev. D* **1995**, *52*, 6882–6893.

[48] D. J. Griffiths, *Introduction to electrodynamics; 4th ed.* Re-published by Cambridge University Press in 2017, Pearson, Boston, MA, **2013**.

[49] P. Fitzpatrick, *Maxwell's Equations and the Principles of Electromagnetism*, Infinity Science Press, **2008**.

[50] B. P. Abbott et al., "Tests of general relativity with the binary black hole signals from the LIGO-Virgo catalog GWTC-1", *Phys. Rev. D* **2019**, *100*, 104036.

[51] C. Van Den Broeck, "Probing dynamical spacetimes with gravitational waves", *Springer Handbook of Spacetime* **2014**, 589–613.

[52] C. Cutler, É. E. Flanagan, "Gravitational waves from merging compact binaries: How accurately can one extract the binary's parameters from the inspiral waveform?", *Phys. Rev. D* **1994**, *49*, 2658–2697.

[53] J. Veitch, A. Vecchio, "Bayesian coherent analysis of in-spiral gravitational wave signals with a detector network", *Phys. Rev. D* **2010**, *81*, 062003.

[54] J. Skilling, "Nested sampling for general Bayesian computation", *Bayesian Analysis* **2006**, *1*, 833–859.

[55] C. van den Broeck, Lectures on Bayesian model selection and parameter estimation, International Centre for Theoretical Sciences, **2015**.

[56] LIGO Scientific Collaboration, LIGO Algorithm Library - LALSuite, free software (GPL), **2018**.

[57] P. Schmidt, M. Hannam, S. Husa, "Towards models of gravitational waveforms from generic binaries: A simple approximate mapping between precessing and nonprecessing inspiral signals", *Phys. Rev. D* **2012**, *86*, 104063.

[58] S. Khan, S. Husa, M. Hannam, F. Ohme, M. Pürrer, X. J. Forteza, A. Bohé, "Frequency-domain gravitational waves from nonprecessing black-hole binaries. II. A phenomenological model for the advanced detector era", *Phys. Rev. D* **2016**, *93*, 044007.

[59] M. Hannam, P. Schmidt, A. Bohé, L. Haegel, S. Husa, F. Ohme, G. Pratten, M. Pürrer, "Simple Model of Complete Precessing Black-Hole-Binary Gravitational Waveforms", *Phys. Rev. Lett.* **2014**, *113*, 151101.

[60] L. Junior, C. Vallio, B. Saragiotto, L. Costa, "Understanding and interpreting confidence and credible intervals around effect estimates", *Brazilian Journal of Physical Therapy* **2019**, *23*, 290–301.

[61] V. Cardoso, C. F. B. Macedo, P. Pani, V. Ferrari, "Black holes and gravitational waves in models of minicharged dark matter", *JCAP* **2016**, *05*, 054.

[62] M. Kramer, "General relativity with double pulsars", *eConf* **2004**.

[63] A. Lyne et al., "A Double-Pulsar System: A Rare laboratory for relativistic gravity and plasma physics", *Science* **2004**, *303*, 1153–1157.

[64] M. Kramer et al., "Tests of general relativity from timing the double pulsar", *Science* **2006**, *314*, 97–102.

[65] T. Damour, J. H. Taylor, "Strong-field tests of relativistic gravity and binary pulsars", *Phys. Rev. D* **1992**, *45*, 1840–1868.

[66] D. R. Lorimer, "Binary and millisecond pulsars", *Living Rev. Rel.* **2005**, *8*, 7.

[67] S. G. Djorgovski, "Kepler's Laws, Binaries, and Stellar Masses", California Institute for Technology, **2004**.

[68] E. Barausse, N. Yunes, K. Chamberlain, "Theory-Agnostic Constraints on Black-Hole Dipole Radiation with Multiband Gravitational-Wave Astrophysics", *Phys. Rev. Lett.* **2016**, *116*, 241104.

[69] N. Yunes, F. Pretorius, "Fundamental Theoretical Bias in Gravitational Wave Astrophysics and the Parameterized Post-Einsteinian Framework", *Phys. Rev. D* **2009**, *80*, 122003.

[70] N. Yunes, S. A. Hughes, "Binary pulsar constraints on the parametrized post-Einsteinian framework", *Phys. Rev. D* **2010**, *82*, 082002.

[71] R. N. Manchester, M. Kramer, A. Possenti, A. G. Lyne, M. Burgay, I. H. Stairs, A. W. Hotan, M. A. McLaughlin, D. R. Lorimer, G. B. Hobbs, J. M. Sarkissian, N. D'Amico, F. Camilo, B. C. Joshi, P. C. C. Freire, "The Mean Pulse Profile of PSR J0737-3039A", *The Astrophysical Journal* **2005**, *621*, L49–L52.

[72] M. Punturo et al., "The Einstein Telescope: A third-generation gravitational wave observatory", *Class. Quant. Grav.* **2010**, *27*, 194002.

[73] C. L. Rodriguez, B. Farr, W. M. Farr, I. Mandel, "Inadequacies of the Fisher information matrix in gravitational-wave parameter estimation", *Phys. Rev. D* **2013**, *88*, 084013.

[74] M. Vallisneri, "Use and abuse of the Fisher information matrix in the assessment of gravitational-wave parameter-estimation prospects", *Phys. Rev. D* **2008**, *77*, 042001.

[75] B. Sathyaprakash et al., "Scientific Potential of Einstein Telescope", *46th Rencontres de Moriond on Gravitational Waves and Experimental Gravity* **2011**, 127–136.